

1 **Arctic Climate Feedback Response to Local Sea-Ice Concentration and**
2 **Remote Sea Surface Temperature Changes in PAMIP Simulations**

3
4 Matthew T. Jenkins* ¹, Aiguo Dai ¹, Clara Deser ²

5
6 ¹University at Albany, State University of New York, Albany, NY, USA

7 ²National Center for Atmospheric Research, Boulder, CO, USA

8
9 Submitted to: *Climate Dynamics*

10 Date: December 22, 2023

11
12
13
14
15
16
17
18
19
20
21
22
23 *Corresponding Author: Matthew T. Jenkins (mtjenkins@albany.edu); ORCID: 0000-0001-5279-1893

24
25
26
27
28
29
30
31
32
33
34
35
36
37
38
39
40
41
42
43
44
45
46
47
48
49
50
51

Abstract

Local and remote processes have been suggested to drive Arctic amplification (AA) – the enhanced warming of the Arctic region relative to other areas under increased greenhouse gases. We use Polar Amplification Model Intercomparison Project (PAMIP) simulations with changes in Arctic sea-ice with fixed global sea surface temperature (SST), or changes in global SST with fixed Arctic sea-ice to untangle the climate response to Arctic sea-ice loss or SST-induced warming, respectively. In response to Arctic sea-ice loss, the surface albedo feedback activates in summer mainly to increase oceanic heat uptake, leading to weak summertime warming. During winter, Arctic sea-ice loss greatly enhances oceanic heat release, which produces Arctic bottom-heavy warming and triggers positive lapse rate and cloud feedbacks, leading to large AA. In contrast, enhanced atmospheric energy convergence into the Arctic becomes the dominant contributor to relatively small AA under global SST-induced warming. Water vapor feedback contributes to Arctic warming but opposes AA due to larger tropical than Arctic moistening under SST-induced warming with fixed Arctic sea-ice. We also find top-heavy to uniform (bottom-heavy) Arctic warming and moistening in the Arctic mid-upper (lower) troposphere in the SST (Arctic sea-ice) perturbation runs, producing a negative-neutral (positive) Arctic lapse rate feedback, respectively. Lastly, we show that the responses to global SST or polar SIC perturbations are linearly separable. Our results suggest that large AA is caused primarily by sea-ice loss and resultant local changes in surface fluxes, while increased poleward energy transport can only produce weak AA under fixed sea ice.

Keywords: Arctic amplification; sea-ice loss; climate feedback; global warming; Arctic warming; ocean heat release; atmospheric energy transport

52 **1. Introduction**

53 The Arctic region warms faster than the rest of the world in response to increased
54 greenhouse gas (GHG) concentrations – a phenomenon known as Arctic amplification (AA)
55 (Serreze and Barry 2011; Walsh 2014; England et al. 2021; Taylor et al. 2022). Many mechanisms
56 have been proposed to explain AA such as surface albedo feedback (Hall 2004; Winton 2006),
57 enhanced poleward energy transport (Cai 2005; Henry et al. 2021), increased surface downwelling
58 longwave (LW) radiation (Burt et al. 2016; Gong et al. 2017), Arctic positive lapse rate feedback
59 (Pithan and Mauritsen 2014; Goosse et al. 2018), and sea-ice loss (Deser et al. 2010; Kumar et al.
60 2010; Screen and Simmonds 2010a, b; Boeke and Taylor 2018; Dai et al. 2019). The local and
61 remote mechanisms suggested to contribute to AA are tightly coupled (Feldl et al. 2017b; Henry
62 et al. 2021; Dai and Jenkins 2023), making the exact causes of AA unclear in a fully coupled
63 system. For instance, sea-ice loss and the spatial patterns of surface warming largely shape Arctic
64 positive lapse rate feedback (Feldl et al. 2020; Boeke et al 2021; Jenkins and Dai 2021). Further,
65 warming in low-mid latitude regions influences Arctic mid-upper tropospheric warming through
66 changes in atmospheric energy convergence into the Arctic, affecting the structure of Arctic
67 warming profiles and lapse rate feedback (Perlwitz et al. 2015; Feldl et al. 2020; Hay et al. 2022).
68 Thus, more work is needed to understand how local and remote processes influence Arctic
69 warming and AA.

70 Arctic sea-ice loss plays an essential role in local Arctic warming (Dai et al. 2019; Linke
71 et al. 2023b) and may contribute to warmer winters in northern hemisphere mid-latitude areas (Sun
72 et al. 2016). Additionally, Arctic sea-ice loss may weaken the stratospheric polar vortex, which
73 can affect weather patterns in the midlatitudes (Liang et al. 2023). As sea-ice retreats, increased
74 energy transfer from warm, open water surfaces to the frigid overlying atmosphere during polar
75 night contributes to large AA (Kumar et al. 2010; Deser et al. 2010; Screen and Simmonds 2010a,
76 b; Boeke and Taylor 2018; Taylor et al. 2018; Dai et al. 2019; Dai and Jenkins 2023). Specifically,
77 Dai et al. (2019) showed that AA weakens in model experiments with 1%/year CO₂ increases and
78 fixed SIC for surface flux calculations, and that negligible additional AA will occur after sea-ice
79 completely melts away. Davy and Griewank (2023) confirmed this finding by showing that as the
80 rate of sea-ice loss decreases in the future, concurrent AA weakens.

81 Another process underlying AA is the lapse rate feedback that depends on local vertical
82 warming structures (Pithan and Mauritsen 2014; Linke et al. 2023a; Zhou et al. 2023). Under a
83 bottom-heavy warming profile, outgoing LW radiation at the top of the atmosphere (TOA) is
84 reduced relative to vertically uniform warming, thereby enhancing surface warming (Boeke et al.
85 2021; Dai and Jenkins 2023). In contrast, a top-heavy warming profile, as seen in the tropics,
86 suppresses surface warming by increasing outgoing LW radiation (Colman and Soden 2021). The
87 lapse rate feedback has been considered as a major contributor to AA due to its large Arctic versus
88 tropical warming effect (Pithan and Mauritsen 2014; Goosse et al. 2018; Hahn et al. 2021).
89 Previous studies have attributed Arctic bottom-heavy warming and the resultant positive lapse rate
90 feedback to high lower-tropospheric stability, which effectively traps warming at the surface
91 (Bintanja et al. 2011; Pithan and Mauritsen 2014). However, recent studies suggest that Arctic
92 lapse rate feedback is strongly correlated with surface warming patterns and sea-ice loss (Feldl et
93 al. 2020; Boeke et al. 2021; Jenkins and Dai 2021) rather than stability strength (Jenkins and Dai
94 2022; Dai and Jenkins 2023). Remote processes, such as enhanced moist static energy convergence
95 into the Arctic, may also influence Arctic lapse rate feedback by favoring warming in the mid-
96 upper troposphere (Feldl et al. 2020), leading to negative lapse rate feedback.

97 During summer, surface albedo and water vapor feedbacks activate in the Arctic in
98 response to greenhouse gas (GHG) forcing. The surface albedo feedback makes a large positive
99 contribution to Arctic energy imbalance in summer (Hall 2004; Winton 2006; Pithan and
100 Mauritsen 2014; Goosse et al. 2018; Hahn et al. 2021); however, most of the enhanced shortwave
101 (SW) absorption preferably warms the ocean mixed layer rather than near-surface air (Dai 2021;
102 Dai and Jenkins 2023). Additionally, water vapor feedback has been suggested to contribute to
103 Arctic *warming* (Ghatak and Miller 2013; Gong et al. 2017) but oppose Arctic *amplification* due
104 to larger moistening in tropical regions than polar areas under increased GHGs (Pithan and
105 Mauritsen 2014; Hahn et al. 2021). Jenkins and Dai (2022) showed that water vapor feedback and
106 sea-ice loss spatial patterns are weakly correlated in ERA5 reanalysis data, but they did not
107 quantify the underlying local and remote drivers of Arctic water vapor feedback. An improved
108 understanding of Arctic water vapor feedback is needed as it enhances Arctic surface warming and
109 melts sea ice, indirectly contributing to AA through the sea-ice feedback (Dai et al. 2019; Dai and
110 Jenkins 2023). Moreover, water vapor feedback may interact with other processes by changing

111 patterns of atmospheric latent energy transport (Chung and Feldl 2023) or amplifying other climate
112 feedbacks (Beer and Eisenman 2022).

113 Cloud feedback impacts TOA and surface energy fluxes (Wetherald and Manabe 1988),
114 but their response to local and remote processes is not fully understood. Previous studies have
115 found an increase in local Arctic low cloud amounts and cloud water content in response to local
116 sea-ice loss due to strong cold season ocean-atmosphere coupling (Schweiger et al. 2008; Kay and
117 Gettelman 2009; Eastman and Warren 2010; Liu et al. 2012; Taylor et al. 2015; Kay et al. 2016;
118 Morrison et al. 2018, 2019; Jenkins and Dai 2022; Jenkins et al. 2023; Taylor and Monroe 2023).
119 Increased surface downwelling LW radiation from local Arctic cloud increases slows sea ice
120 growth during Arctic autumn and winter, lengthening exposure of open water surfaces to heat the
121 overlying air during the cold season (Monroe et al. 2021). Nonlocal cloud feedbacks may also
122 contribute to Arctic warming and AA by affecting remote surface warming patterns and thus
123 atmospheric energy transport into the Arctic (Vavrus et al. 2004; Middlemas et al. 2020).

124 Increased energy transport from midlatitudes into the Arctic has been suggested to
125 influence AA (Cai 2005; Roe et al. 2015; Feldl et al. 2017b; Soldatenko 2021). Without sea-ice
126 loss and associated surface heating, enhanced poleward atmospheric energy transport produces
127 only weak AA in model simulations (Alexeev et al. 2005; Merlis and Henry 2018; Henry et al.
128 2021). On the other hand, inclusion of sea-ice loss effects in model simulations reduces
129 atmospheric energy transport into the Arctic due to decreased temperature gradients between
130 middle and high latitudes (Hwang et al. 2011; Jenkins and Dai 2021; Hahn et al. 2023). Further,
131 Cardinale and Rose (2023) showed that an increase in the fraction of the Arctic energy
132 convergence used to heat the surface may overcome the total decrease in Arctic energy
133 convergence, contributing to winter Arctic warming. Inhomogeneous spatial patterns of radiative
134 forcing also influence atmospheric poleward energy transport (Stuecker et al. 2018; Virgin and
135 Smith 2019). When radiative forcing is negative in the Arctic, atmospheric poleward energy
136 transport increases to offset the energy imbalance, inducing small AA (Virgin and Smith 2019).
137 Additionally, Stuecker et al. (2018) found that atmospheric energy transport became an important
138 contributor to AA in response to radiative forcing applied only in midlatitudes in fully coupled
139 simulations, but they did not examine the effects of sea-ice loss in shaping the Arctic warming in
140 response to such forcing.

141 The relative importance of sea-ice loss, positive climate feedbacks, and atmospheric energy
142 transport in shaping AA is still debated and merits further investigation. Arctic climate feedbacks
143 have been estimated in coupled model simulations (Pithan and Mauritsen 2014; Goosse et al. 2018;
144 Stuecker et al. 2018; Previdi et al. 2020; Hahn et al. 2021); however, the influence of local sea-ice
145 loss or remote SST warming on climate feedbacks cannot be explicitly quantified in a fully coupled
146 system. To address these points, we use atmosphere-only simulations from the Polar Amplification
147 Model Intercomparison Project (PAMIP; Smith et al. 2019) to answer the following questions:

- 148 1. What are the impacts of local Arctic SIC changes through enhanced oceanic heating of the
149 atmosphere or global SST changes and background warming in atmosphere-only model
150 simulations on Arctic surface warming, AA, radiative climate feedbacks, and atmospheric
151 energy transport?
- 152 2. Do the individual responses to SST warming or Arctic SIC loss sum to the total response
153 to the combined influences of SST warming and Arctic SIC loss occurring simultaneously?

154 The PAMIP experiments allow us to separate the climate response to perturbations in local sea ice
155 or remote SST changes in model simulations under fixed GHG concentrations. The SST
156 perturbation runs represent the climatic effects of background global warming without large AA,
157 while the Arctic SIC change simulations show the impact from Arctic sea-ice loss without
158 background global warming.

159 **2. Methods**

160 *2.1 PAMIP experiments*

161 We investigate how changes in global SST and/or local SIC impact Arctic surface
162 warming, AA, climate feedbacks, and atmospheric energy transport using PAMIP atmosphere-
163 only time slice experiments (Table 1; Smith et al. 2019). PAMIP experiment 1.1 (pdSST-pdSIC)
164 serves as the control run where global SST and polar (i.e., Arctic and Antarctic) SIC fields are
165 fixed at their present-day (pd) (i.e., year 2000) values. To isolate the response to global SST
166 changes, we compare the pdSST-pdSIC run to PAMIP experiments 1.3 (piSST-pdSIC) and 1.4
167 (futSST-pdSIC) where polar (i.e., Arctic and Antarctic) SIC remains fixed at present-day
168 conditions and SSTs over open water surfaces are set to preindustrial (pi) and future (fut) states
169 (defined below), respectively. Likewise, we difference the pdSST-pdSIC run with PAMIP

170 experiments 1.5 (pdSST-piArcSIC) and 1.6 (pdSST-futArcSIC) where SSTs outside the Arctic
 171 region are fixed at their present-day values and Arctic SIC is changed to preindustrial and future
 172 states to separate the impacts of sea-ice loss from other forcings. For the pdSST-piArcSIC and
 173 pdSST-futArcSIC simulations, SSTs are specified at their preindustrial or future values in regions
 174 where preindustrial or future SIC deviates by more than 10% of the present-day state, respectively
 175 (Smith et al. 2019).

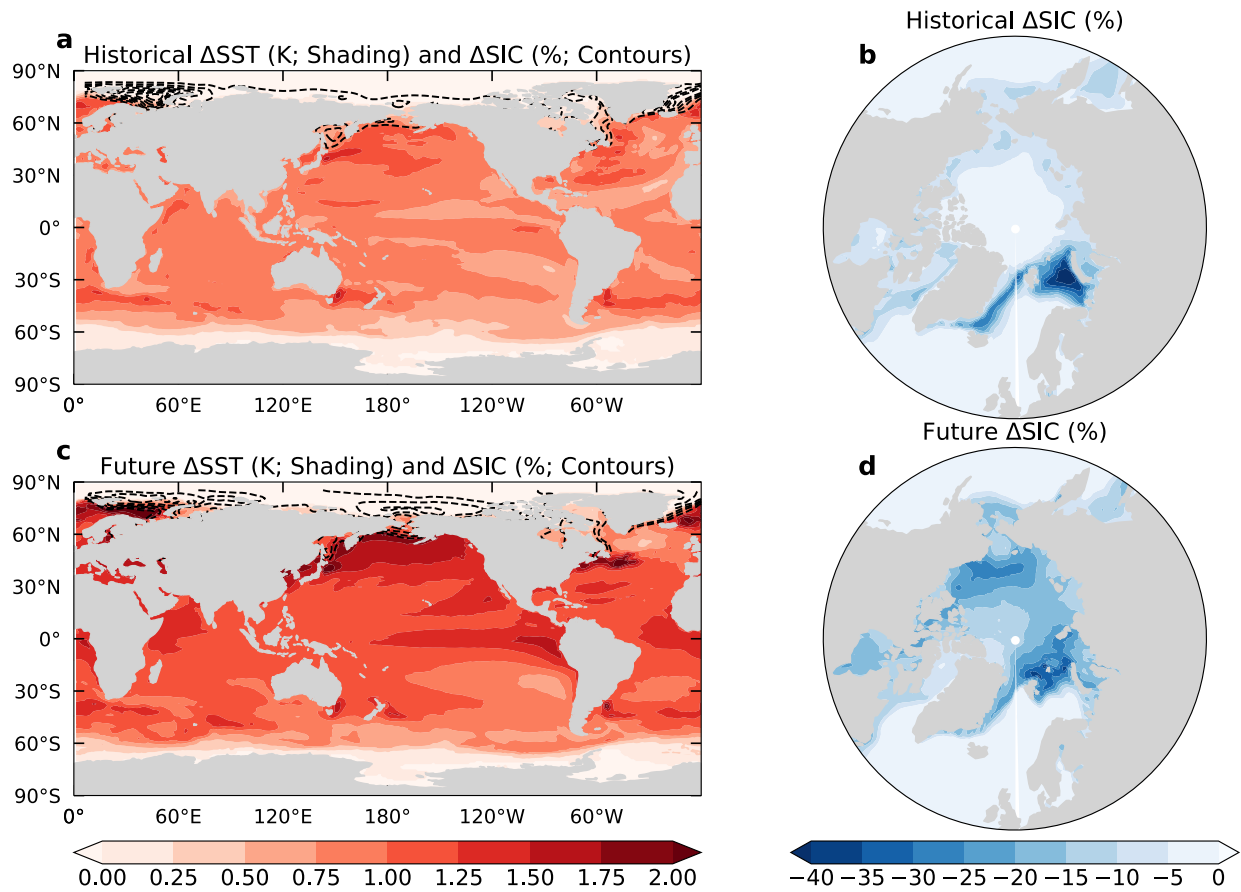
176 Figure 1 shows the maps of prescribed SST and SIC changes for the preindustrial (Fig. 1a,
 177 b) or future (Fig. 1c, d) cases. To facilitate comparison with the future changes, which are relative
 178 to present-day, the historical changes are computed as present-day minus preindustrial in Fig. 1
 179 and all other figures. We also compute the difference between pdSST-pdSIC and experiment 1.2
 180 (piSST-piSIC; referred to as TOTAL) where global SSTs and polar SIC are changed
 181 simultaneously to their preindustrial states. We compare the results from the piSST-piSIC run to
 182 the sum of piSST-pdSIC, pdSST-piArcSIC and pdSST-piAntSIC (referred to as SUM) simulations
 183 to assess the linearity of the total climate response to both polar SIC and global SST changes. The
 184 preindustrial, present-day, and future time periods correspond to estimated Arctic SIC and/or
 185 global SST conditions under global-mean surface temperatures of 13.67°C, 14.24°C, and 15.67°C,
 186 respectively (Smith et al. 2019), which correspond to a historical warming of 0.57°C and a future
 187 warming of 1.43°C relative to present-day. Their corresponding SIC changes are also much larger
 188 for the future case than the historical case (Fig. 1).

189 **Table 1.** Summary of PAMIP experiments used in the analysis (from Smith et al. 2019).

Model Simulation	Full Name	Description
1.1 pdSST-pdSIC	Present day sea surface temperature Present-day sea-ice concentration	Year 2000 global SST and polar SIC; control run.
1.2 piSST-piSIC	Preindustrial sea surface temperature Preindustrial sea-ice concentration	Historical global SST and polar SIC; assesses total climate response to SST and SIC changes.
1.3 piSST-pdSIC	Preindustrial sea surface temperature Present-day sea-ice concentration	Historical (1.3) and future (1.4) global SST with polar SIC fixed at year 2000 conditions; assesses role of background warming without sea-ice feedback.
1.4 futSST-pdSIC	Future sea surface temperature Present-day sea-ice concentration	

1.5 pdSST-piArcSIC	Present-day sea surface temperature Preindustrial sea-ice concentration	Historical (1.5) and future (1.6) Arctic SIC with global SST fixed at year 2000 conditions; assesses role of Arctic sea-ice feedback without background warming.
1.6 pdSST-futArcSIC	Present-day sea surface temperature Future sea ice concentration	
1.7 pdSST-piAntSIC	Present-day SST Preindustrial Antarctic SIC	Historical Antarctic SIC with global SST fixed at year 2000 conditions; assesses role of Antarctic sea-ice feedback without background warming.

190



191

192 **Fig. 1.** (a, c) Annual mean changes in SST (K; shading) and Arctic SIC (%; contours; interval 5%)
 193 for the (a) historical (present-day minus preindustrial) and (c) future warming (future minus
 194 present-day) cases. Changes in SIC for the (b) historical and (d) future cases are shown as shading
 195 in (b) and (d) for clarity.

196 We use monthly-mean output from five models (i.e., AWI-CM1-1-MR, CESM2, CNRM-
197 CM6-1, CanESM5, IPSL-CM6A-LR) that provided the necessary fields for our analysis. AWI-
198 CM1-1-MR and CNRM-CM6-1 did not output the necessary variables for some calculations in
199 piSST-piSIC (i.e., TOTAL) and is excluded in our comparison of piSST-piSIC to the sum of
200 piSST-pdSIC, pdSST-piArcSIC, and pdSST-piAntSIC (i.e., SUM). Each model and experiment
201 are initialized on 1 April 2000 and are run for 14-months, discarding the first two months as spin-
202 up (Smith et al. 2019). To improve robustness of the results, we analyze the ensemble mean of the
203 100 ensemble runs with varied initial conditions for each model and experiment as atmospheric
204 internal variability can mask the climatic response to SIC or SST changes (Screen et al. 2014). We
205 define the Arctic region as the area poleward of 67°N following previous work (e.g., Dai et al.
206 2019; Jenkins and Dai 2022) because most Arctic sea-ice exists poleward of this latitude and the
207 Arctic is mostly ocean surface in this region. We exclude land surfaces in our Arctic regional
208 averages because surface warming is strongest over oceanic areas (Boeke and Taylor 2018; Dai et
209 al. 2019) but inclusion of land areas does not qualitatively affect our results. Globally averaged
210 fields include both land and ocean surfaces. For this study, we calculate AA as the difference
211 between Arctic (excluding land) and global surface air temperature (ΔT_{as}) changes ($AA =$
212 $\Delta T_{as,ARCTIC} - \Delta T_{as,GLOBAL}$) rather than as the ratio of Arctic to global warming to avoid dividing by
213 near-zero values for global-mean surface air temperature changes.

214 2.2 Energy budgets

215 The vertically integrated energy budget equation (Eq. 1) for an atmospheric column
216 accounts for the net TOA radiative flux (R_{TOA}^\downarrow ; positive downward), net surface energy flux (R_{SFC}^\downarrow ;
217 positive downward), change in local energy storage in the atmospheric column ($\frac{\partial E}{\partial t}$), and horizontal
218 convergence of energy ($-\nabla \cdot \mathbf{F}_A$) (Trenberth 1997; Fasullo and Trenberth 2008):

$$219 \quad \frac{\partial E}{\partial t} = R_{TOA}^\downarrow - R_{SFC}^\downarrow - \nabla \cdot \mathbf{F}_A \quad , \quad (1)$$

220 where

$$221 \quad E = \frac{1}{g} \int_{p_{TOA}}^{p_s} (c_p T + Lq + gz) dp. \quad (2)$$

222 In Eq. (2), E is the vertically integrated moist static energy, where $c_p T$, Lq , and gz denote
223 atmospheric internal energy, latent energy, and potential energy, respectively. Atmospheric kinetic

224 energy storage is small and is not included in Eq. (2), following previous studies (Oort and Vonder
 225 Haar 1976; Trenberth and Solomon 1994). For the flux terms, we calculate R_{TOA}^{\downarrow} and R_{SFC}^{\downarrow} as:

$$226 \quad R_{TOA}^{\downarrow} = ASR^{\downarrow} - OLR^{\uparrow} \quad (3)$$

$$227 \quad R_{SFC}^{\downarrow} = SW_{NET,SFC}^{\downarrow} - LW_{NET,SFC}^{\uparrow} - SH^{\uparrow} - LH^{\uparrow} \quad (4)$$

228 where ASR^{\downarrow} , OLR^{\uparrow} , $SW_{NET,SFC}^{\downarrow}$, $LW_{NET,SFC}^{\uparrow}$, SH^{\uparrow} , and LH^{\uparrow} are the TOA absorbed SW radiation
 229 (positive downward), TOA outgoing LW radiation (positive upward), net surface SW radiation
 230 (positive downward), net surface LW radiation (positive upward), surface sensible and latent heat
 231 flux (positive upward), respectively. To estimate oceanic heat uptake (OHU), we calculate the net
 232 surface energy flux (Eq. 4) over ocean surfaces only.

233 We compute the horizontal atmospheric energy convergence ($-\nabla \cdot \mathbf{F}_A$) by rearranging the
 234 terms in Eq. (1) to obtain:

$$235 \quad -\nabla \cdot \mathbf{F}_A = R_{SFC}^{\downarrow} - R_{TOA}^{\downarrow} + \frac{\partial E}{\partial t}. \quad (5)$$

236 Eq. (5) shows that the net convergence of the horizontal energy flux (in $W m^{-2}$) into a column is
 237 linked to the difference between the energy absorbed at the surface and net TOA radiation, and
 238 changes in local energy storage. We also calculate the atmospheric energy transport (AET; in PW)
 239 into the region north of a given latitude (ϕ) by taking the area integral of the net energy convergence
 240 over the region following previous studies (Hwang and Frierson 2010; Feldl et al. 2017a):

$$241 \quad AET(\phi) = \int_{\phi}^{\pi/2} \int_0^{2\pi} \left(R_{SFC}^{\downarrow} - R_{TOA}^{\downarrow} + \frac{\partial E}{\partial t} \right) a^2 \cos \phi \, d\gamma d\phi. \quad (6)$$

242 In Eq. (6), a is the radius of Earth ($\sim 6.371 \times 10^6$ m), γ is the longitude, and ϕ is the latitude.
 243 $AET(\phi)$ represents the total energy crosses the latitude circle at ϕ (positive northward). For our
 244 Arctic region, $\phi=67^{\circ}N$.

245 *2.3 Climate feedback calculations*

246 The response of the atmospheric energy budget to a climate perturbation, assuming
 247 negligible changes in atmospheric energy storage, is:

$$248 \quad \Delta R_{TOA}^{\downarrow} - \Delta R_{SFC}^{\downarrow} - \Delta(\nabla \cdot \mathbf{F}_A) = 0 \quad (7)$$

249 where $\Delta R_{TOA}^\downarrow$, $\Delta R_{SFC}^\downarrow$, and $\Delta(\nabla \cdot \mathbf{F}_A)$ are changes in the net TOA radiative flux, net surface energy
 250 flux, and atmospheric horizontal energy convergence at each grid point, respectively (Stuecker et
 251 al. 2018; Hahn et al. 2021; Zhou et al. 2023). We use the Pendergrass et al. (2018) CESM1-CAM5
 252 radiative kernels to decompose changes in the TOA net radiative flux into individual contributions
 253 from changes in surface albedo (ΔR_α), air temperature (ΔR_T), water vapor (ΔR_q), and clouds (ΔR_C):

$$254 \quad \Delta R_{TOA}^\downarrow = \Delta R_\alpha^\downarrow + \Delta R_q^\downarrow + \Delta R_T^\downarrow + \Delta R_C^\downarrow. \quad (8)$$

255 GHG concentrations remain fixed at year 2000 levels in the PAMIP simulations, so we exclude an
 256 effective radiative forcing term from our TOA flux change decomposition. We also normalize the
 257 TOA flux changes in Eq. (8) by the local surface air temperature change (ΔT_{as}) to calculate the
 258 climate feedback parameter (λ_i) for each variable using:

$$259 \quad \sum_i \lambda_i = \lambda_\alpha + \lambda_q + \lambda_T + \lambda_C = \frac{\Delta R_\alpha^\downarrow + \Delta R_q^\downarrow + \Delta R_T^\downarrow + \Delta R_C^\downarrow}{\Delta T_{as}} \quad (9)$$

260 For clarity, we use the term *feedback* to refer to the unnormalized TOA radiative flux changes
 261 (units: W m^{-2}) in Eq. (8) and *feedback parameter* to refer to the normalized TOA radiative fluxes
 262 (units: $\text{W m}^{-2} \text{K}^{-1}$) in Eq. (9).

263 Radiative kernels are computed by perturbing one climate variable in a radiative transfer
 264 model and keeping all other variables fixed to produce a TOA radiative flux response, which is
 265 divided by the amount of the perturbed variable change to derive the TOA flux change per unit
 266 variable change (Soden et al. 2008). To calculate the surface albedo feedback, we compute the
 267 product of the surface albedo kernel (K_α) and changes in surface albedo ($\Delta\alpha$): $\Delta R_\alpha = K_\alpha * \Delta\alpha$. For
 268 water vapor (Eq. 10) and temperature (Eq. 11) feedbacks, we vertically integrate the product of
 269 the kernel and change in each respective variable from the surface (p_s) to the tropopause (p_{TOA}):

$$270 \quad \Delta R_q = \int_{p_{TOA}}^{p_s} K_q * \Delta \ln(q) dp \quad (10)$$

$$271 \quad \Delta R_T = \int_{p_{TOA}}^{p_s} K_{T_a} * \Delta T_a dp \quad (11)$$

272 where q and T_a represent specific humidity and air temperature, respectively. Radiative emissions
 273 from water vapor scale with the natural logarithm of specific humidity, so we use $\Delta \ln(q)$ in Eq.
 274 (11) as done previously (Shell et al. 2008). Further, we assume that the tropopause pressure
 275 increases with latitude from 100 hPa at the equator to 300 hPa at the poles following Pithan and

276 Mauritsen (2014) to mask out the stratosphere. To calculate Planck and lapse rate feedbacks, we
 277 separate the temperature feedback (ΔR_T) into a component associated with vertically uniform
 278 warming equal to that of the surface (Planck feedback; ΔR_{PL}) and deviations from the vertically
 279 uniform warming profile (lapse rate feedback; ΔR_{LR}):

$$280 \quad \Delta R_T = \Delta R_{LR} + \Delta R_{PL} = \int_{p_{TOA}}^{p_s} K_{T_a} * (\Delta T_a - \Delta T_{as}) dp + \int_{p_{TOA}}^{p_s} K_{T_a} * \Delta T_{as} dp \quad (12)$$

281 More details on Planck and lapse rate feedback calculations are provided in Dai and Jenkins
 282 (2023).

283 The change in cloud radiative forcing (ΔCRF) – the difference between all-sky and clear-
 284 sky radiative fluxes – provides a simple estimate of the energetic effects of clouds but does not
 285 represent cloud feedback as other processes also affect this difference (Soden et al. 2008; Block
 286 and Mauritsen 2013). To compute cloud feedback (ΔR_C), we subtract a cloud masking (CM) term
 287 from the ΔCRF to account for the effects of changes in surface albedo, temperature, and water
 288 vapor on ΔCRF (Soden et al. 2008):

$$289 \quad \Delta R_C = \Delta CRF - CM \quad (13)$$

290 where

$$291 \quad CM = (K_\alpha - K_\alpha^C) * \Delta\alpha + \int_{p_{TOA}}^{p_0} (K_{T_a} - K_{T_a}^C) * \Delta T_a dp + \int_{p_{TOA}}^{p_0} (K_q - K_q^C) * \Delta l n(q) dp. \quad (14)$$

292 In Eq. (14) K_i and K_i^C are the all-sky and clear-sky kernels for surface albedo (α), air temperature
 293 (T_a), and water vapor (q). GHG concentrations are fixed in the PAMIP runs so we exclude a GHG
 294 masking term in Eq. (14).

295 *2.4 Potential warming contribution estimates*

296 To facilitate comparison, we quantify climate feedbacks, oceanic heat uptake, and
 297 horizontal atmospheric energy convergence in terms of their *potential* warming contributions
 298 following previous studies (e.g., Pithan and Mauritsen 2014; Goosse et al. 2021; Stuecker et al.
 299 2018; Hahn et al. 2021). The potential warming contribution from the i th climate feedback ($\Delta T_i = \Delta R_i$
 300 $/\bar{\lambda}_{PL}$, in K) represents a hypothetical warming amount needed to rebalance the TOA energy flux
 301 change ($\Delta R_i = \lambda_i \Delta T_{as}$) through the negative Planck feedback at a new *equilibrium* state. Similarly,

302 we can scale the other flux changes to estimate their potential warming contributions, and the total
 303 potential warming amount (ΔT) is estimated as (Goosse et al. 2018; Hahn et al. 2021):

$$304 \quad \Delta T = -\frac{\sum_i \lambda_i \Delta T_{as}}{\bar{\lambda}_{PL}} - \frac{\lambda'_{PL} \Delta T_{as}}{\bar{\lambda}_{PL}} - \frac{\Delta(-\nabla \cdot \mathbf{F}_A)}{\bar{\lambda}_{PL}} - \frac{\Delta OHU}{\bar{\lambda}_{PL}} \quad (15)$$

305 where $\bar{\lambda}_{PL}$ (in $\text{W m}^{-2} \text{K}^{-1}$) is the global-mean Planck feedback parameter and λ'_{PL} is the deviation of
 306 the local (λ_{PL}) Planck feedback parameter from its global mean: $\lambda'_{PL} = \lambda_{PL} - \bar{\lambda}_{PL}$. As noted by
 307 Dai and Jenkins (2023), this estimated warming amount often does not represent a real warming
 308 contribution as the TOA flux change (ΔR_i) may not be used to directly raise surface air temperature
 309 or the temperature response may be delayed. We average the terms in Eq. (15) over the Arctic
 310 ($67^\circ\text{-}90^\circ\text{N}$) and the tropics ($23.5^\circ\text{S}\text{-}23.5^\circ\text{N}$) to estimate the potential warming contribution of each
 311 process to surface warming and AA as done previously (Pithan and Mauritsen 2014; Goosse et al.
 312 2018; Stuecker et al. 2018; Hahn et al. 2021).

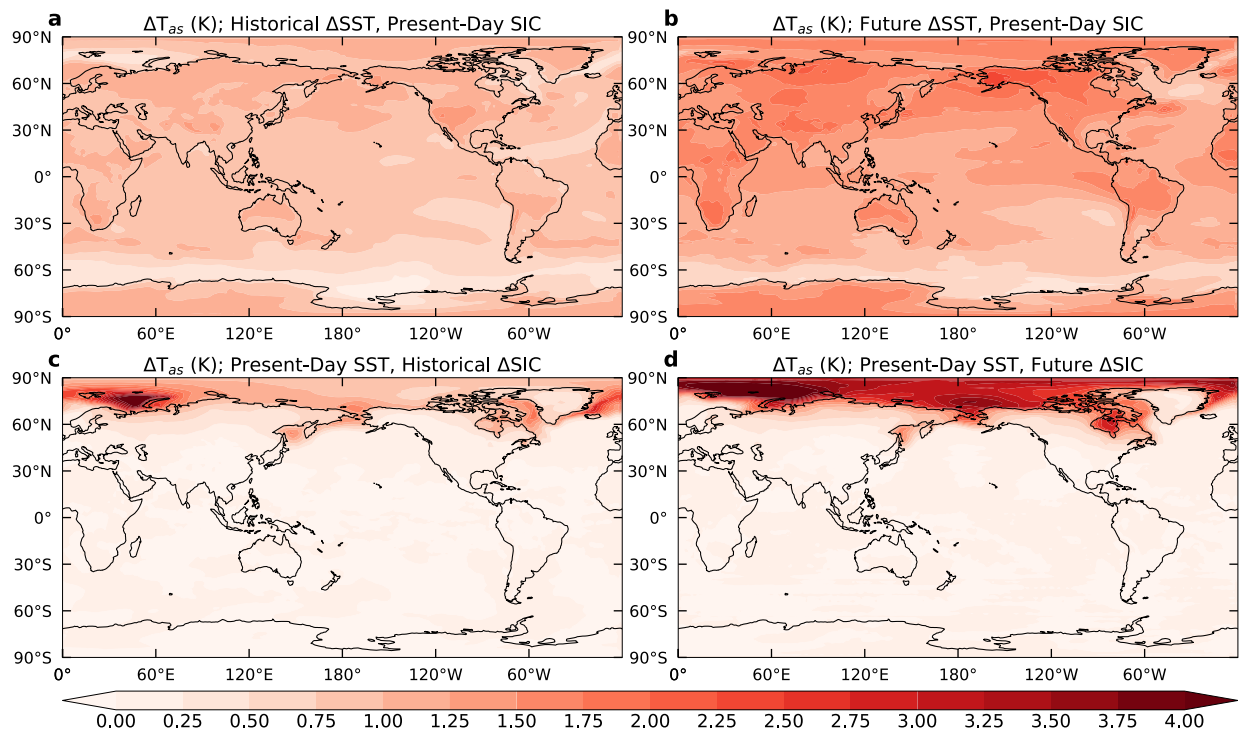
313 **3. Results**

314 *3.1 Surface warming response to changes in global SST or Arctic SIC*

315 We first examine the annual-mean surface air temperature response to historical and future
 316 global SST (Fig. 2a, b) or Arctic SIC (Fig. 2c, d) changes shown in Figure 1. The globe experiences
 317 relatively uniform warming in pdSST-pdSIC relative to piSST-pdSIC (Fig. 2a, referred to as
 318 historical warming) and in futSST-pdSIC relative to pdSST-pdSIC (Fig. 2b, referred to as future
 319 warming), with slightly greater magnitude in the future SST case (around 1.0-2.0 K) than the
 320 historical case (0.5-1.0 K). Thus, the SST perturbation runs show background global warming
 321 without noticeable AA. In contrast, reduced Arctic sea-ice leads to large warming over the Arctic
 322 with little temperature change south of $\sim 60^\circ\text{N}$ in both the historical and future perturbed SIC runs
 323 (Fig. 2b, d). Note that the local Arctic warming is larger for the future case ($\sim 3\text{-}5$ K; Fig. 2d) than
 324 the historical case ($\sim 1\text{-}3$ K; Fig. 2c) as the future sea-ice loss is larger (Fig. 1c-d) and that the
 325 largest historical warming (Fig. 2c) occurs over the Barents-Kara Seas region where there is large
 326 sea-ice loss (Fig. 1b).

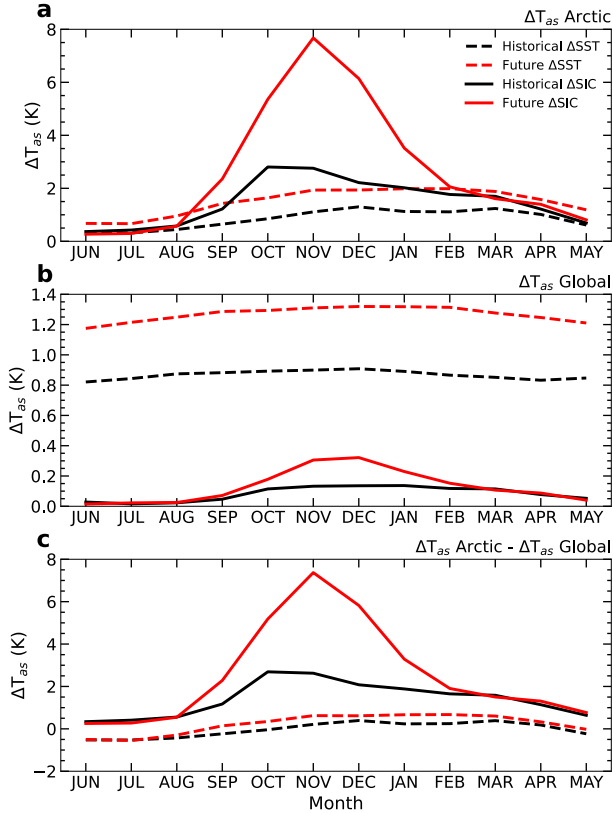
327 The seasonal cycle of the surface air temperature changes averaged over the Arctic (Fig.
 328 3a) and globe (Fig. 3b) shows different responses to global SST or Arctic SIC perturbations. Global
 329 SST perturbations produce small Arctic warming during historical ($\sim 0.5\text{-}1.0$ K) and future ($\sim 1.0\text{-}$

330 2.0 K) periods for October-March and negligible summer warming (Fig. 3a). The global-mean
 331 surface temperature warms by ~ 0.8 K for the historical and ~ 1.2 K for the future SST cases, with
 332 little seasonal variation (Fig. 3b). Thus, there is small AA (< 0.8 K) during October-March while
 333 the summer Arctic warming is weaker than the global-mean warming in the SST perturbation
 334 experiments (Fig. 3c). In contrast, Arctic sea-ice loss produces large Arctic warming from
 335 October-January for the historical (~ 3 K) and future ($\sim 6-8$ K) cases, with weak warming in summer
 336 (Fig. 3a). Note that the peak warming shifts from October in the historical case to November in
 337 the future case. The global-mean warming response to the SIC changes is weak throughout most
 338 of the year except the cold season (Fig. 3b), which is due to the large warming in the Arctic (Fig.
 339 2c-d). As a result, AA is strong from October-January for the two perturbed SIC cases, especially
 340 for the future SIC case (up to 7 K), while the AA is weak (< 1 K) during the summer months (Fig.
 341 3c).



342

343 **Fig. 2.** Multi-model ensemble mean changes in annual-mean surface air temperature (ΔT_{as}) in
 344 response to (a, c) historical and (b, d) future (a, b) SST and (c, d) SIC changes shown in Fig. 1.



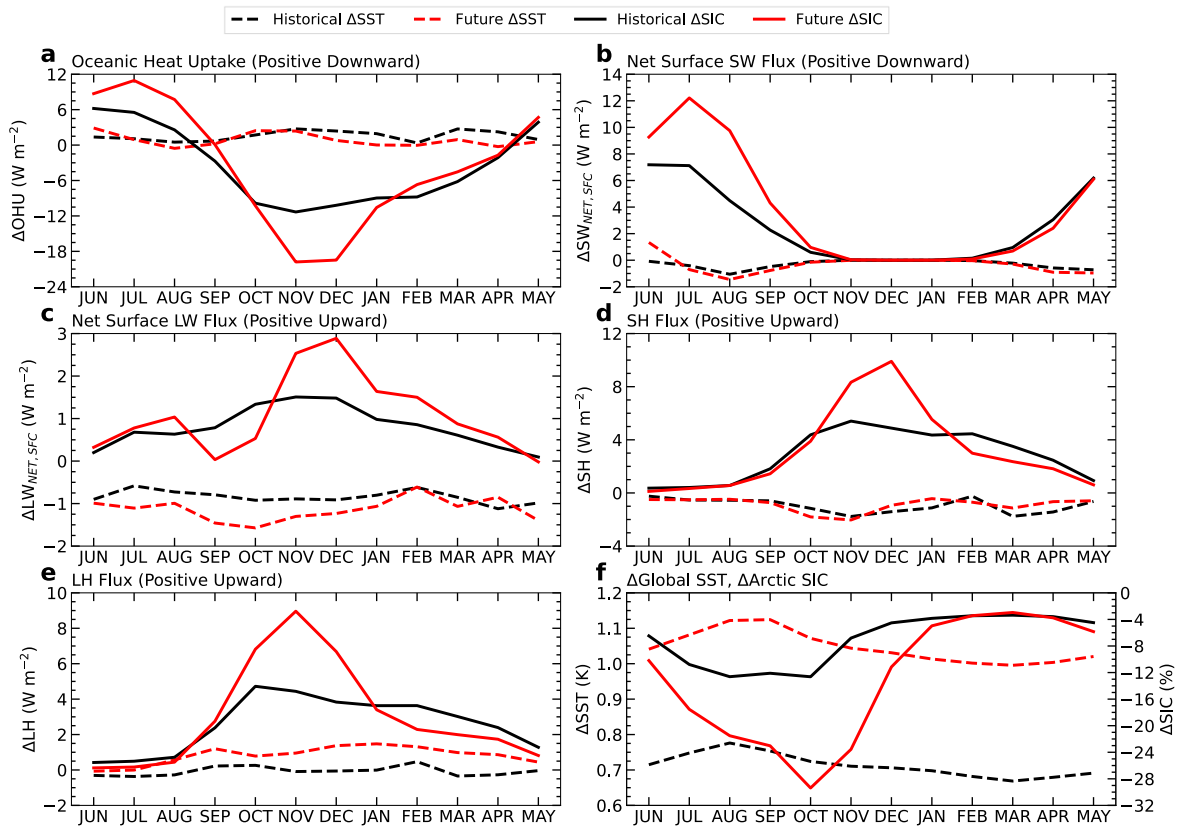
345

346 **Fig. 3.** Multi-model ensemble mean seasonal cycle of surface air temperature changes (ΔT_{as} ; in K)
 347 in response to historical (black lines) and future (red lines) SST (dashed lines) and SIC (solid lines)
 348 perturbations shown in Fig. 1 averaged over the (a) Arctic (67° - 90° N) and (b) globe, and (c) Arctic
 349 minus global-mean difference (i.e., Arctic amplification).
 350

351 3.2 Surface energy budget response to Global SST or local Arctic SIC changes

352 Increased upward surface energy fluxes over sea-ice retreat areas have been shown to drive
 353 large Arctic warming and AA in winter (Deser et al. 2010; Boeke and Taylor 2018; Taylor et al.
 354 2018; Dai et al. 2019). In response to SST warming with fixed SIC, we find little change in the net
 355 surface energy flux, net surface SW, SH, and LH fluxes over the Arctic Ocean throughout the year
 356 (Fig. 4). The upward net surface LW flux decreases by $\sim 1 \text{ W m}^{-2}$ for both the historical and future
 357 SST warming cases with fixed SIC (Fig. 4c). This represents a small increase in the downward
 358 LW radiation, likely due to increased water vapor and enhanced atmospheric energy convergence
 359 into the Arctic, rather than changes to surface conditions, as shown below. The suppressed Arctic
 360 surface warming and weak oceanic energy flux response to SST warming without SIC changes is
 361 consistent with Dai et al. (2019), who found similar results in model simulations with increasing
 362 CO_2 concentrations and fixed Arctic sea-ice in flux calculations.

363 Arctic sea-ice loss greatly influences the magnitude and seasonal cycle of the Arctic
 364 oceanic heat flux. From May-August, oceanic *absorption* of energy increases by $\sim 6\text{-}12\text{ W m}^{-2}$ in
 365 response to historical and future SIC loss (Fig. 4f) while during October-March oceanic *release* of
 366 energy increases by $\sim 12\text{-}18\text{ W m}^{-2}$ (Fig. 4a). Most of the increased oceanic energy absorption from
 367 May-August is due to increased absorption of SW radiation (Fig. 4b), with negligible changes in
 368 net surface LW, SH, and LH fluxes (Fig. 4c-e) during summer. In contrast, net surface LW, SH,
 369 and LH fluxes are the main contributors to the enhanced cold-season oceanic energy release in
 370 response to Arctic sea-ice loss. Specifically, the SH (LH) flux contributes $\sim 4\text{-}6\text{ W m}^{-2}$ ($\sim 3\text{-}4\text{ W m}^{-2}$
 371 2) and $\sim 8\text{-}10\text{ W m}^{-2}$ ($\sim 8\text{-}9\text{ W m}^{-2}$) in response to historical and future SIC loss, respectively (Fig.
 372 4d, e). Further, the ocean surface emits $\sim 1\text{-}2\text{ W m}^{-2}$ ($\sim 1\text{-}3\text{ W m}^{-2}$) more LW radiation to the
 373 atmosphere in autumn and winter in the historical (future) Arctic sea-ice loss runs (Fig. 4c). The
 374 large increases in upward surface energy fluxes in response to sea-ice loss play an important role
 375 in enhancing warming of the surface air and AA during winter (Fig. 3a).
 376



377
 378 **Fig. 4.** Arctic ($67^{\circ}\text{-}90^{\circ}\text{N}$) multi-model ensemble mean seasonal cycle of changes in (a) OHU
 379 (positive downward), (b) net surface SW flux (positive downward), (c) net surface LW flux

380 (positive upward), **(d)** SH flux (positive upward), and **(e)** LH flux (positive upward) in response
381 to historical (black lines) and future (red lines) SST (dashed lines) and SIC (solid lines)
382 perturbations shown in Fig. 1. All values are in W m^{-2} and land surfaces are excluded from
383 averages. **(f)** The seasonal cycle of the historical (black lines) and future (red lines) global SST
384 changes (left y-axis; dashed lines) and Arctic SIC loss (right y-axis; solid lines) specified in the
385 SIC and SST perturbation experiments.

386

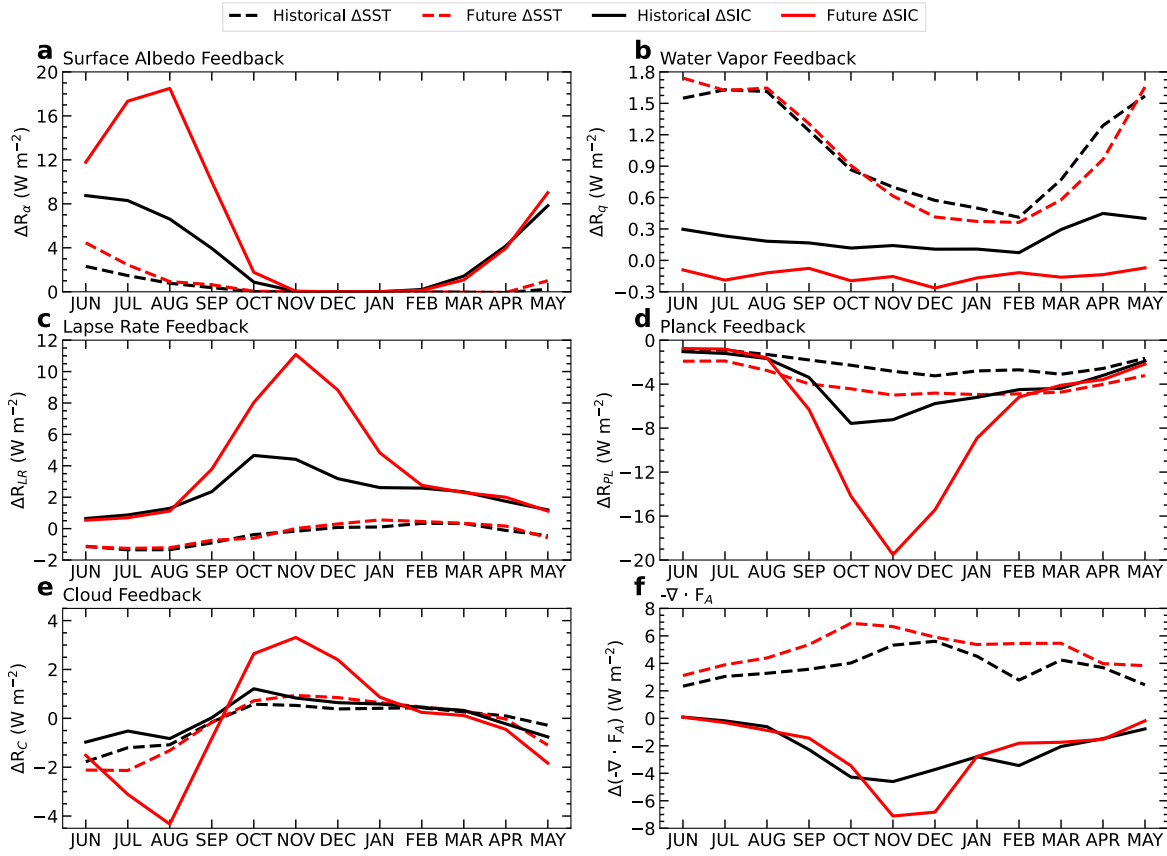
387 *3.3 Feedback seasonal cycles and warming contributions*

388 The contrasting surface warming responses to global SST changes or local sea-ice loss
389 greatly influence Arctic climate feedbacks and atmospheric energy convergence changes. Under
390 global SST warming with fixed SIC, Arctic atmospheric energy convergence (Fig. 5f) and water
391 vapor feedback (Fig. 5b) become important contributors to the Arctic TOA flux change.
392 Specifically, atmospheric energy convergence into the Arctic responds similarly to historical and
393 future SST warming, with increases of $\sim 4\text{-}7 \text{ W m}^{-2}$ during the winter months and $\sim 2\text{-}4 \text{ W m}^{-2}$ in
394 summer (Fig. 5f). This suggests that without changes in sea ice, increased atmospheric energy
395 transport becomes an important contributor to small cold season Arctic warming and AA (Fig. 3).
396 Further, the magnitude and seasonal cycle of the water vapor feedback is similar between the
397 historical and future SST cases, with maximum water vapor feedback ($1.5\text{-}1.8 \text{ W m}^{-2}$) from May-
398 August and minimum water vapor feedback ($0.4\text{-}0.7 \text{ W m}^{-2}$) during October-March (Fig. 5b). This
399 is expected as the warm-season Arctic would see larger water vapor increases due to its warmer
400 mean air temperatures. Arctic surface albedo (Fig. 5a), lapse rate (Fig. 5c), and Planck (Fig. 5d)
401 feedbacks weakly respond to SST increases without sea-ice loss. Lastly, we note that the net cloud
402 feedback produces slight cooling ($-1.5\text{-}2.0 \text{ W m}^{-2}$) in response to SST increases for June-August
403 (Fig. 5e).

404 In response to sea-ice loss, Arctic surface albedo feedback increases by $\sim 7\text{-}8 \text{ W m}^{-2}$ and
405 $\sim 12\text{-}18 \text{ W m}^{-2}$ for historical and future cases during the sunlit months (i.e., April-September) due
406 to increased exposure of dark water surfaces (Fig. 5a). The ocean, rather than the atmosphere,
407 absorbs much of the extra SW radiation (Fig. 4a), resulting in weak summer surface warming (Fig.
408 3a). Cloud feedback is negative in response to sea-ice loss during April-August, and the cooling is
409 larger in the future SIC case ($-1.5\text{-}4.5 \text{ W m}^{-2}$) than the preindustrial SIC run ($-1.0\text{-}1.5 \text{ W m}^{-2}$).
410 Lapse rate (Fig. 5c) and Planck (Fig. 5d) feedbacks weakly respond to historical or future Arctic
411 SIC changes in summer due to small surface warming (Fig. 3a) during the sunlit season. We also

412 find negligible water vapor feedback in response to Arctic sea-ice loss throughout the year, which
413 differs from the noticeable water vapor feedback in response to SST warming (Fig. 5b).

414 The large cold-season surface warming in response to historical and future Arctic sea-ice
415 loss enhances Arctic lapse rate (Fig. 5c) and Planck (Fig. 5d) feedbacks. When Arctic surface
416 warming (Fig. 3a) and AA (Fig. 3c) peak from October-December, the lapse rate feedback
417 increases the incoming TOA radiative flux by $\sim 4\text{-}6\text{ W m}^{-2}$ ($\sim 8\text{-}11\text{ W m}^{-2}$) and the Planck feedback
418 opposes warming by $-6\text{-}8\text{ W m}^{-2}$ ($-16\text{-}20\text{ W m}^{-2}$) due to historical (future) sea-ice loss. Note that
419 the month of maximum (minimum) lapse rate (Planck) feedback in the historical and future SIC
420 cases (Fig. 5c) corresponds to the month of peak Arctic surface warming (Fig. 3a), which in turn
421 is related to peak oceanic heating (Fig. 4a) induced by sea-ice loss (Fig. 4f) in these simulations.
422 The cloud feedback in response to future Arctic sea-ice loss also enhances the net incoming TOA
423 radiative flux from October-January by $\sim 2.5\text{-}3.0\text{ W m}^{-2}$, but the cloud feedback is weak ($<1.0\text{ W}$
424 m^{-2}) during winter in response to historical sea-ice loss (Fig. 5e). In contrast to the SST change
425 simulations, Arctic atmospheric energy convergence weakens by 7 W m^{-2} and $9\text{-}13\text{ W m}^{-2}$ in
426 response to historical and future sea-ice loss from October-January, respectively (Fig. 5f).
427 Enhanced Arctic warming in response to sea-ice loss in the non-summer months (Fig. 3a) weakens
428 the temperature gradient between the midlatitudes and polar regions, thus reducing atmospheric
429 energy convergence into the Arctic region.

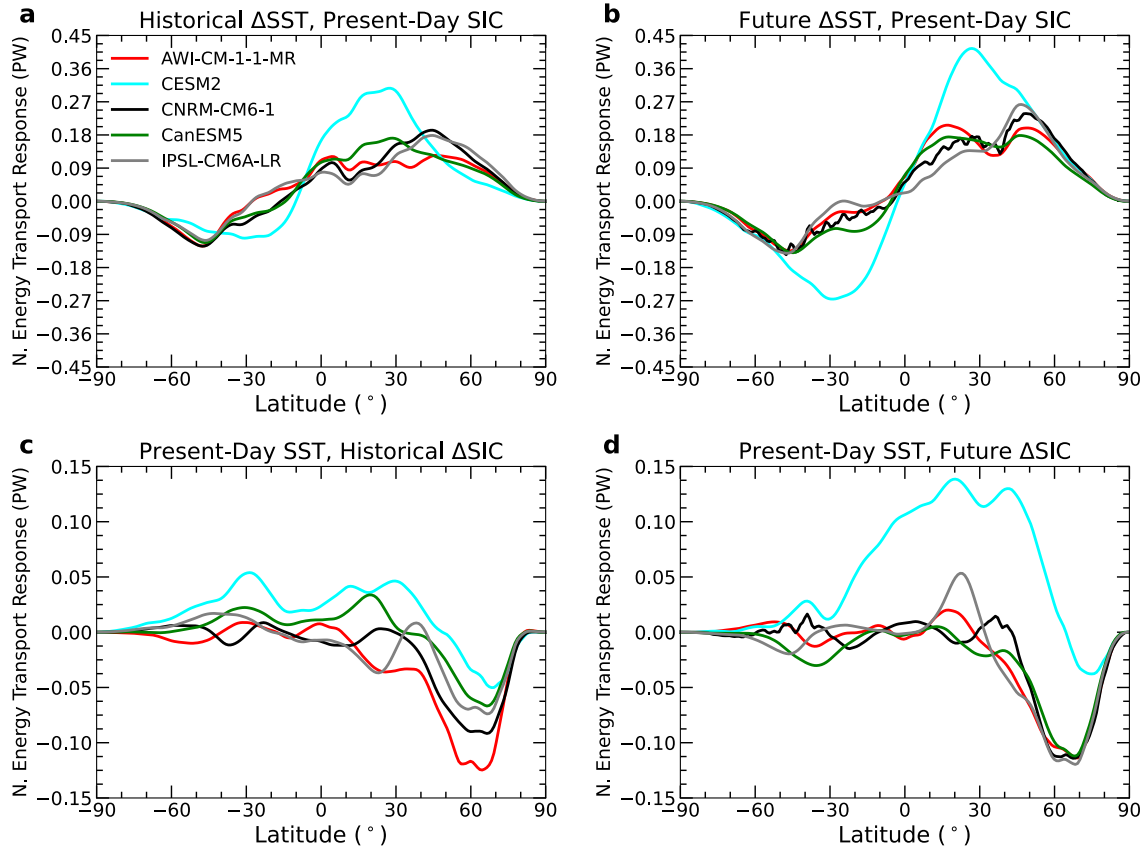


430

431 **Fig. 5.** Arctic (67° - 90° N) multi-model ensemble mean seasonal cycle of the (a) surface albedo,
 432 (b) water vapor, (c) lapse rate, (d) Planck, and (e) cloud feedbacks, and (f) changes in atmospheric
 433 energy convergence into the Arctic in response to historical (black lines) and future (red lines)
 434 SST (dashed lines) and SIC (solid lines) changes shown in Fig. 1. All values are in W m^{-2} and land
 435 surfaces are excluded in averages except for the case shown in (f).
 436

437 Warmer SSTs enhance poleward atmospheric energy transport at all latitudes for each
 438 model for the historical (Fig. 6a) and future (Fig. 6b) SST warming cases, with slightly larger
 439 increases in the northern hemisphere than southern hemisphere from October-March. All models,
 440 except CESM2, show enhanced cold season northward energy transport with peak increases of
 441 ~ 0.18 (~ 0.22) PW around $\sim 45^{\circ}$ - 50° N for the historical (future) SST warming cases. In CESM2,
 442 atmospheric energy transport shows peak increases of 0.27 (0.40) PW around 30° N for October-
 443 March. Thus, without large Arctic warming related to sea-ice loss, the atmosphere displaces energy
 444 surpluses poleward. For the SIC perturbation experiments, there is a net decrease in poleward
 445 atmospheric energy transport around 30° - 90° N with a maximum decrease of -0.05 ~ -0.12 PW
 446 around 60° N but little change south of 30° N for both historical (Fig. 6c) and future (Fig. 6d) sea-
 447 ice loss, consistent with Deser et al. (2015). Therefore, SST-induced background warming

448 enhances atmospheric poleward energy transport into the polar regions, while large Arctic
 449 warming in response to sea-ice loss weakens atmospheric poleward energy transport over the
 450 northern mid-high latitudes.

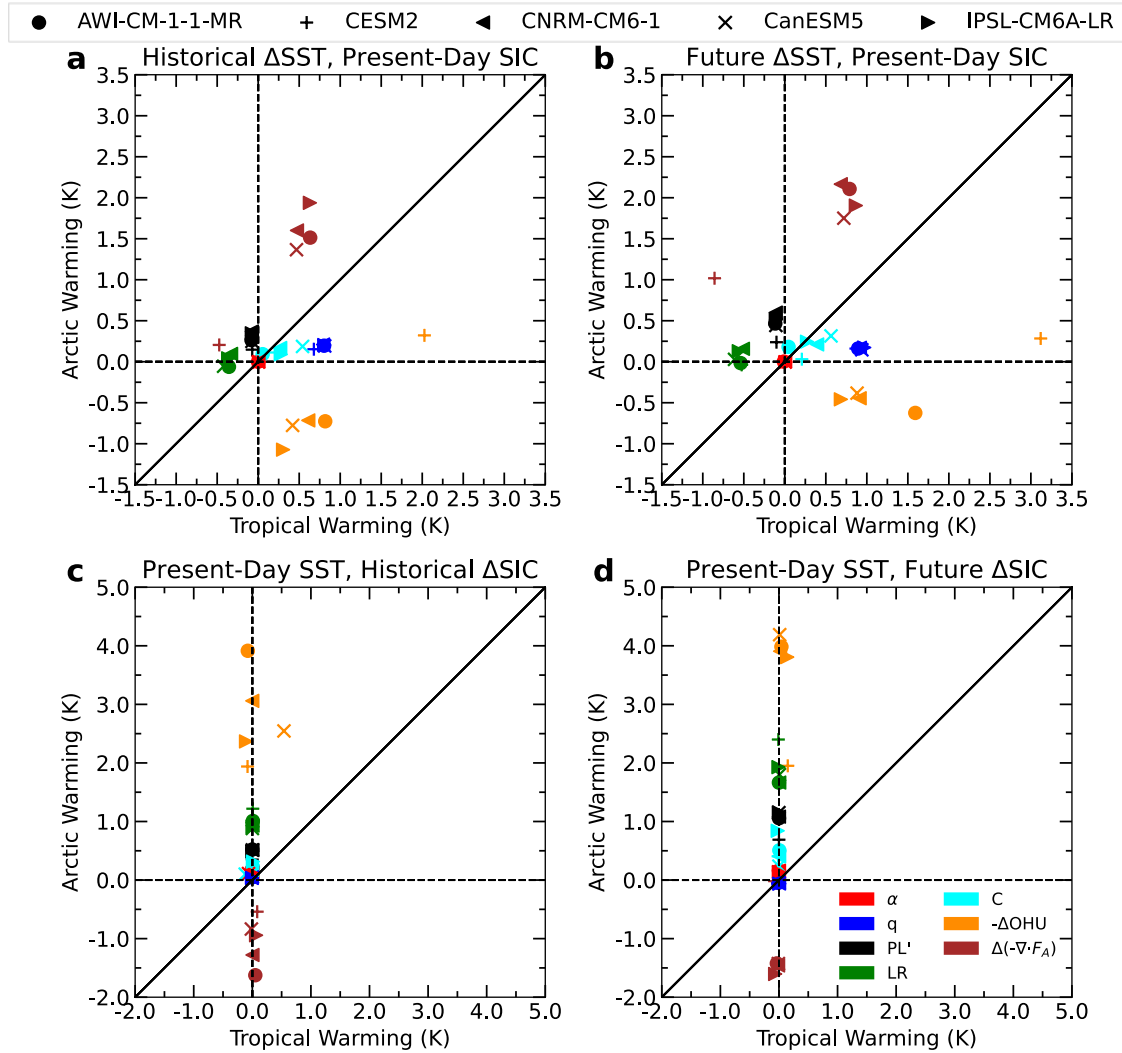


451
 452 **Fig. 6.** Changes in October-March mean Arctic northward energy transport in response to (a, c)
 453 historical and (b, d) future (a, b) SST and (c, d) SIC changes shown in Fig. 1.

454
 455 Figure 7 shows the *potential* warming contributions of the climate feedbacks over the
 456 Arctic and the tropics. A larger (smaller) Arctic than tropical warming contribution indicates that
 457 the process contributes positively (negatively) to AA (Pithan and Mauritsen 2014). We focus on
 458 the warming contributions from October-March (rather than the annual-mean) as surface warming
 459 and AA is largest during the cold season (Fig. 3a) and warm-season positive contributions (such
 460 as that from surface albedo feedback) do not lead to significant surface warming as the energy is
 461 stored in the upper ocean. Atmospheric energy convergence is the largest contributor to cold-
 462 season AA under historical (Fig. 7a) and future (Fig. 7b) global SST warming, as it redistributes

463 the energy from the lower latitude oceans, where SSTs increase, to the Arctic region. In contrast,
464 oceanic heat release opposes AA in response to global SST warming (Fig. 7a-b) because the
465 warmer SSTs produce a greater ocean-to-atmosphere energy flux outside the Arctic, thus causing
466 more warming in the tropics than in the Arctic. Water vapor feedback makes a small contribution
467 to Arctic warming due to low October-March mean temperatures but contributes to ~ 1 K of
468 warming in the tropics in response to global SST warming (Fig. 7b), opposing AA. Without sea-
469 ice loss, lapse rate feedback contributes little to Arctic warming but produces weak tropical cooling
470 in response to historical (Fig. 7a) and future (Fig. 7b) SST increases from October-March. The
471 local Planck feedback (relative to the global-mean Planck feedback) slightly contributes to AA in
472 the SST warming runs because the cooling effects from Planck feedback are slightly less in the
473 Arctic region than over the rest of the world (Fig. 7a-b). Surface albedo and cloud feedbacks
474 contribute little to Arctic warming or AA in response to global SST increases and fixed Arctic SIC
475 during October-March for historical (Fig. 7a) and future (Fig. 7b) cases.

476 In response to Arctic sea-ice loss with fixed global SSTs, oceanic heat release is the largest
477 contributor to AA from October-March in historical (Fig. 7c) and future (Fig. 7d) SIC cases,
478 followed by the positive lapse rate feedback. This supports previous studies that showed that sea-
479 ice loss and oceanic energy release during Arctic winter are necessary to trigger large surface
480 warming and thus strong positive lapse rate feedback in the Arctic (Feldl et al. 2020; Jenkins and
481 Dai 2021; Dai and Jenkins 2023). The local Planck feedback (relative to the global-mean Planck
482 feedback) also contributes to Arctic warming and AA in response to historical (Fig. 7c) and future
483 (Fig. 7d) Arctic SIC changes by cooling the Arctic region less than the tropics. Additionally,
484 positive cloud feedback makes a slight contribution to cold-season Arctic warming and AA in
485 response to future Arctic SIC loss (Fig. 7d), but the contribution is negligible in the historical SIC
486 loss run (Fig. 7c). Water vapor feedback is suppressed over the Arctic and globe in the historical
487 (Fig. 7c) and future (Fig. 7d) SIC runs, suggesting that local sea-ice loss and water vapor feedback
488 are decoupled, as found previously (Jenkins and Dai 2021). In contrast to the perturbed SST runs,
489 the atmosphere displaces energy away from the Arctic in response to cold season sea-ice loss (Fig.
490 7c-d), thus opposing AA.



491

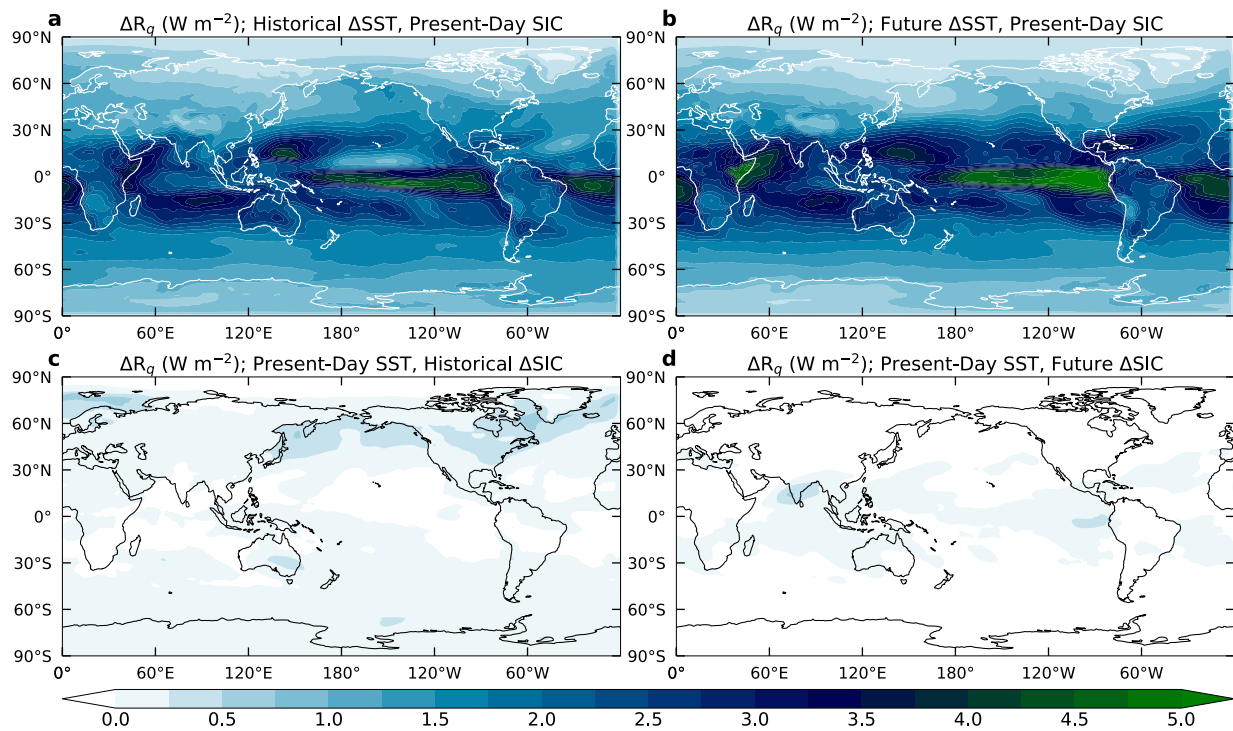
492 **Fig. 7.** Inter-model spread in ensemble mean, October-March *potential* warming contributions (in
 493 K) of Arctic (67°-90°N) vs. tropical (23.5°S-23.5°N) surface albedo (α), water vapor (q), Planck
 494 (PL'), lapse rate (LR), and cloud (C) feedbacks, and changes in oceanic heat release ($-\Delta\text{OHU}$;
 495 positive upwards), and atmospheric energy convergence ($\Delta(-\nabla \cdot \mathbf{F}_A)$) in response to (a, c)
 496 historical and (b, d) future (a, b) SST and (c, d) SIC perturbations shown in Fig. 1.

497

498 3.4 Physical processes underlying climate feedbacks

499 Water vapor feedback is complicated in high latitudes due to local temperature inversions
 500 and low amounts of water vapor (Curry et al. 1995; Sejas et al. 2018). Global maps reveal that
 501 SST warming (Fig. 8a, b) has a larger effect than local sea-ice loss (Fig. 8c, d) on water vapor
 502 feedback in both the Arctic and remote areas. Specifically, water vapor feedback is largest near

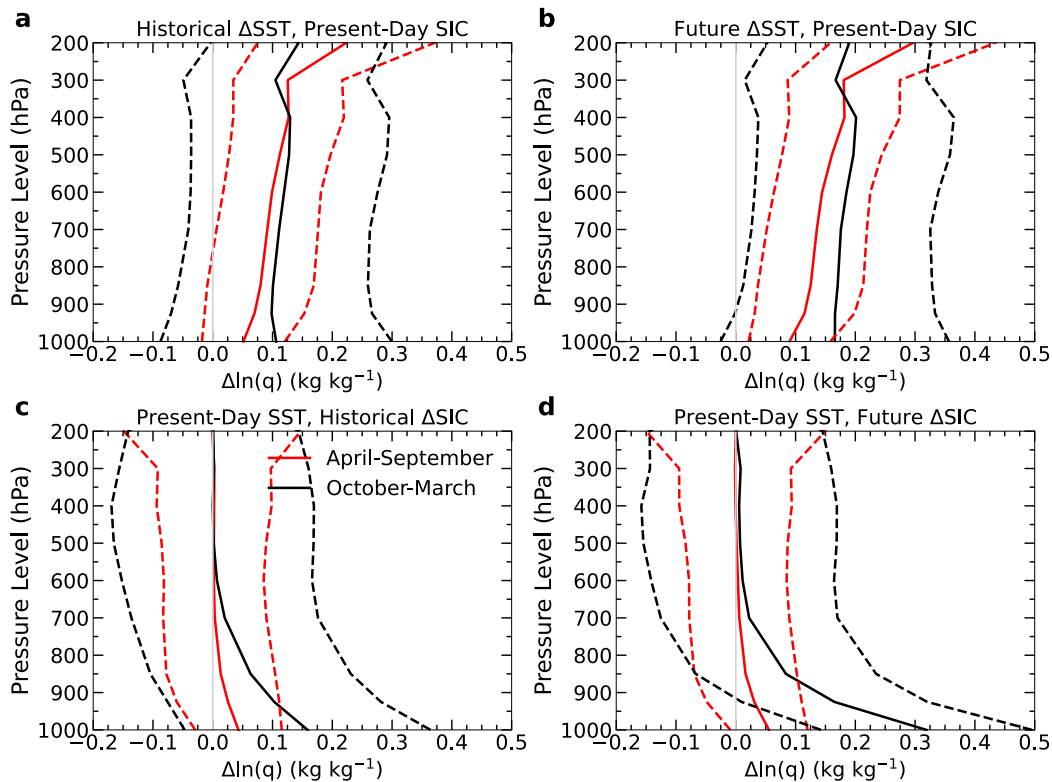
503 the equator at $\sim 2\text{-}5 \text{ W m}^{-2}$ in response to historical (Fig. 8a) and future (Fig. 8b) SST warming and
 504 decreases poleward to $\sim 0.5\text{-}1.0 \text{ W m}^{-2}$ in the Arctic region (Fig. 8a, b). The cold-season water
 505 vapor feedback is weak in response to Arctic sea-ice loss (Fig. 8c, d), including over the Arctic
 506 where low-level specific humidity increases (Fig. 9c, d). This is due to low or negative values of
 507 the October-March LW and net (i.e., LW+SW) water vapor kernel in the Arctic lower troposphere
 508 (Fig. 10a, c). Because the water vapor feedback is most sensitive to upper tropospheric water vapor
 509 content (Shell et al. 2008; Soden et al. 2008; Pendergrass et al. 2018), the low-level water vapor
 510 increases in response to Arctic sea-ice loss do not lead to large TOA flux changes.



511
 512 **Fig. 8.** Multi-model ensemble mean October-March water vapor feedback (in W m^{-2}) in response
 513 to (a, c) historical and (b, d) future (a, b) SST and (c, d) SIC changes shown in Fig. 1.

514
 515 Slight positive water vapor feedback occurs over sea-ice loss areas in the historical SIC
 516 loss run ($\sim 0.50\text{-}0.75 \text{ W m}^{-2}$; Fig. 8c) but there are negligible water vapor feedback effects in the
 517 Arctic under future SIC conditions (Fig. 8d). As the October-March LW and net water vapor kernel
 518 is negative near the surface (Fig. 10a, c), any increase in moisture in the lower troposphere will
 519 result in enhanced radiative emission to space (i.e., a negative water vapor radiative effect). In
 520 response to future Arctic SIC (Fig. 9d), there are greater increases in the natural logarithm of
 521 specific humidity [$\Delta \ln(q)$] in the lower troposphere than in the historical case (Fig. 9c). Thus,

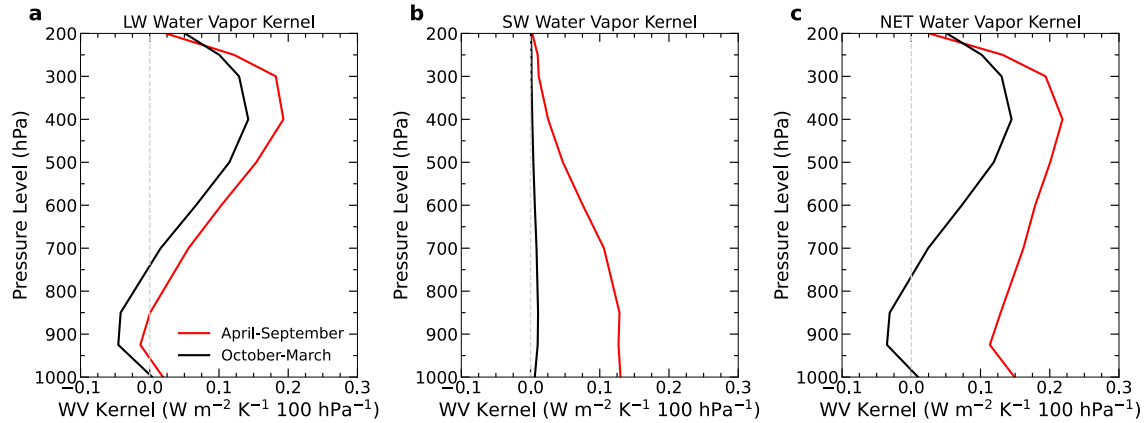
522 greater future lower tropospheric moistening in the Arctic region produces a more negative water
 523 vapor radiative effect at the TOA. We also note that there is a large spread (as shown by the
 524 standard deviation) among the PAMIP models and individual ensemble members in upper
 525 tropospheric moistening in the perturbed Arctic SIC runs, where there is little change in the mean
 526 $\Delta \ln(q)$ (Fig. 10c, d). Thus, some ensemble members may have experienced a slight decrease in
 527 upper tropospheric $\Delta \ln(q)$ in response to Arctic sea-ice loss with fixed global SST, enhancing
 528 outgoing LW radiation at the TOA. In contrast, the historical (Fig. 10a) and future (Fig. 10b)
 529 perturbed SST runs experienced slightly greater $\Delta \ln(q)$ in the upper troposphere than the lower
 530 troposphere for both warm and cold seasons. Due to positive values of the TOA LW and net Arctic
 531 water vapor kernel in the upper troposphere (Fig. 10a, c), top-heavy moistening in response to
 532 global SST warming produces a positive water vapor feedback from the TOA perspective.



533

534 **Fig. 9.** Multi-model, ensemble mean (solid lines) Arctic (67° - 90° N; land surfaces excluded)
 535 changes in the natural logarithm of specific humidity (in kg kg^{-1} ; solid lines) in response to (a, c)
 536 historical and (b, d) future (a, b) SST and (c, d) SIC changes shown in Fig. 1. Dashed lines show
 537 ± 1 standard deviation from the multi-model ensemble mean profile.

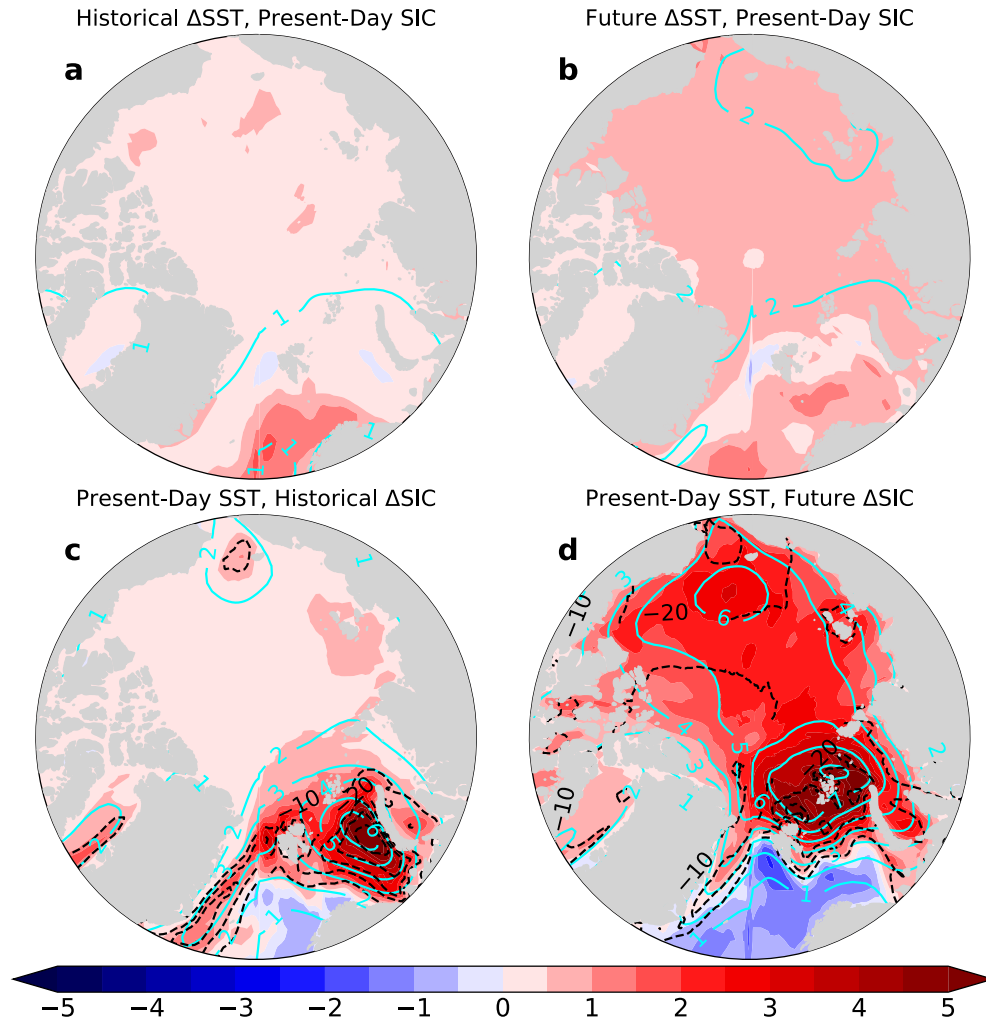
538



539

540 **Fig. 10.** Profiles of the Pendergrass et al. (2018) TOA (a) LW, (b) SW, and (c) NET (LW+SW)
 541 water vapor kernel (in $W m^{-2} K^{-1} 100 hPa^{-1}$) averaged over the Arctic region (67° - $90^{\circ}N$).
 542

543 Arctic low cloud amount has been suggested to increase during the cold season in response
 544 to sea-ice loss due to decreased lower tropospheric stability (Kay and Gettelman 2009; Jenkins et
 545 al. 2023), thus affecting Arctic cloud feedback (Vavrus 2004; Morrison et al. 2019; Jenkins and
 546 Dai 2022). We find weak October-March cloud feedback in response to perturbed SST with fixed
 547 Arctic SIC for historical (Fig. 11a) and future (Fig. 11b) cases, suggesting that remote processes
 548 do not greatly impact Arctic cloud feedback. On the other hand, Arctic sea-ice loss produces a
 549 large positive cloud feedback response in winter, especially in regions with large sea-ice loss and
 550 surface warming (Fig. 11c, d). For the run with historical SIC loss, cloud feedback enhances the
 551 TOA radiative flux by ~ 2 - $5 W m^{-2}$ in the Barents-Kara Seas region and by ~ 0.5 - $1.0 W m^{-2}$ in the
 552 Chukchi Sea, where the largest sea-ice loss and surface warming occurs. Under future Arctic sea-
 553 ice loss, cold-season cloud feedback is largest in the Barents-Kara Seas (~ 3 - $5 W m^{-2}$) except the
 554 warming effects from clouds extend into the Central Arctic Ocean. This is likely related to the
 555 greater area with large sea-ice loss (Fig. 1b, d) and surface warming (Fig. 2c-d) in the future case
 556 than in the historical case.



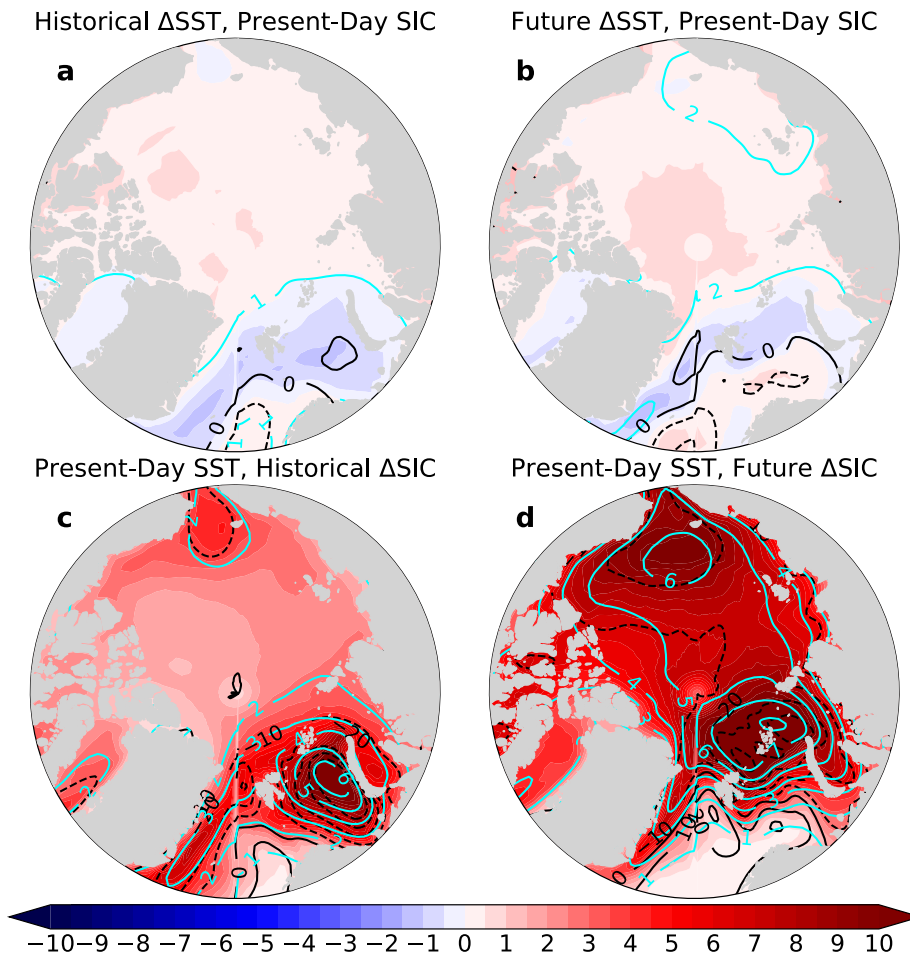
557

558 **Fig. 11.** Multi-model ensemble mean TOA radiative flux change due to the cloud feedback
 559 (shading; in W m^{-2}) and change in surface air temperature (cyan contours; in K) averaged over
 560 October-March in response to (a, c) historical and (b, d) future (a, b) SST and (c, d) SIC changes.
 561 Black contours in (c) and (d) show the change in Arctic SIC for October-March.

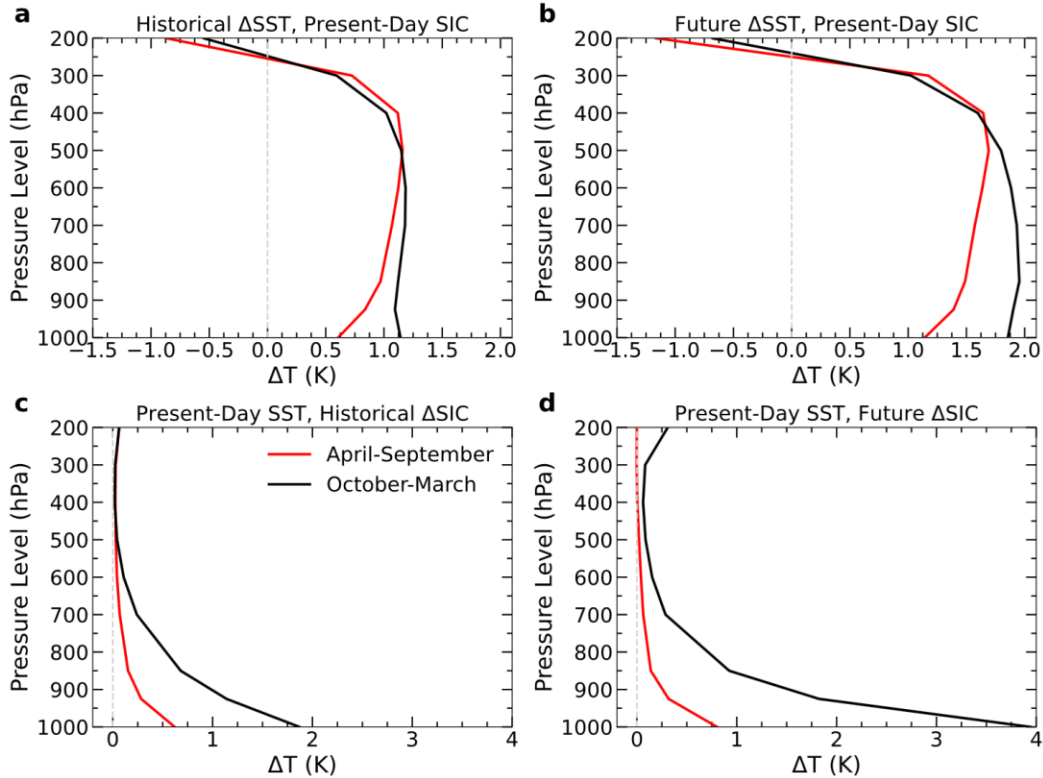
562

563 The lapse rate feedback experiences large seasonal and spatial variations in the Arctic in
 564 response to SST warming or Arctic SIC loss. From October-March, the lapse rate feedback is
 565 negative-neutral in response to the global SST warming (Fig. 12a, b) due to relatively uniform
 566 vertical warming profiles (Fig. 13a, b). We note that without changes in SIC, there are negligible
 567 changes in Arctic oceanic heat uptake or surface warming in the cold season, leading to suppressed
 568 lapse rate feedback (Fig. 12a, b). In contrast, cold-season sea-ice loss enhances Arctic lapse rate
 569 feedback for historical (Fig. 12c) and future (Fig. 12d) SIC cases when surface and lower

570 tropospheric warming outpaces warming in the mid-upper troposphere (Fig. 13c, d). We note that
 571 lapse rate feedback strengthens ($\sim 6\text{-}10 \text{ W m}^{-2}$) in regions with the greatest October-March oceanic
 572 heat release and surface warming in response to historical (Fig. 12c) and future (Fig. 12d) sea-ice
 573 loss, consistent with previous studies (Dai et al. 2019; Feldl et al. 2020; Boeke et al. 2021; Jenkins
 574 and Dai 2021, 2022; Dai and Jenkins 2023). Thus, sea-ice loss is necessary to produce bottom-
 575 heavy warming and trigger Arctic positive lapse rate feedback during winter, as shown previously
 576 by Dai and Jenkins (2023) using coupled model experiments.



577
 578 **Fig. 12.** Multi-model, ensemble mean TOA radiative flux change due to the lapse rate feedback
 579 (shading; in W m^{-2}), changes in oceanic heat uptake (black contours; in W m^{-2} ; positive
 580 downward), and changes in surface air temperature (cyan contours; in K) averaged over October-
 581 March in response to (a, c) historical and (b, d) future (a, b) SST and (c, d) SIC changes.
 582



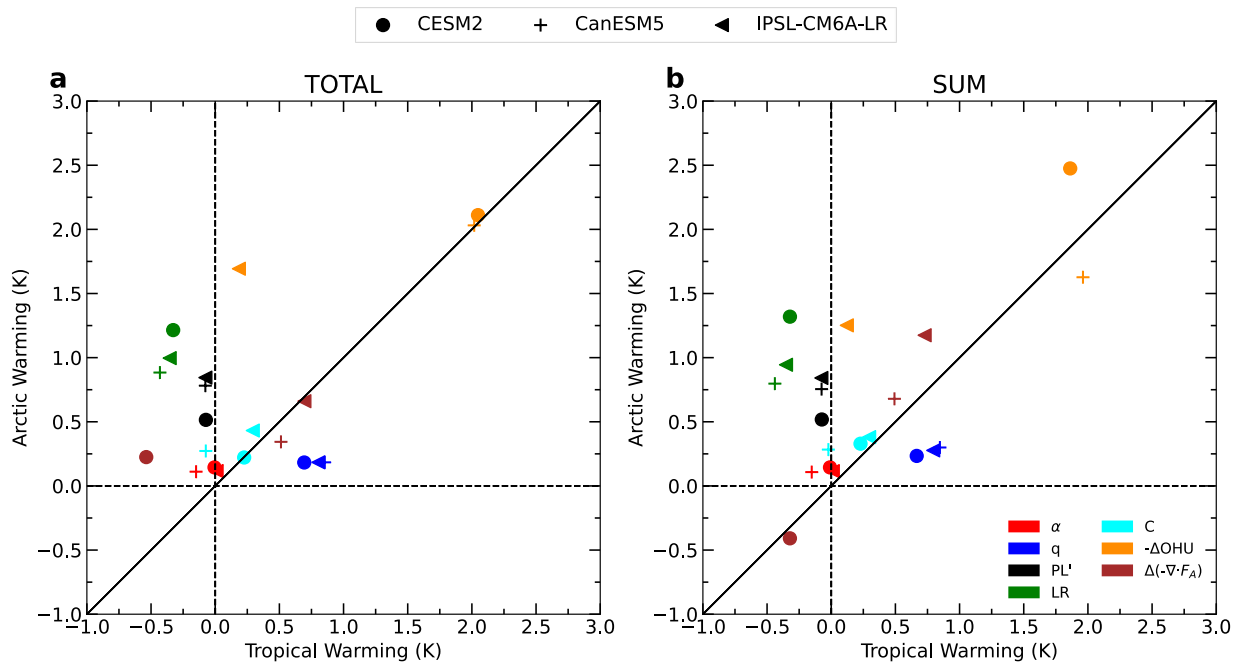
583
584
585
586
587
588

Fig. 13. Multi-model, ensemble mean Arctic (67° - 90° N; land surfaces excluded) temperature change profiles (in K) averaged over April-September (red lines) and October-March (black lines) in response to the (a) historical and (b) future global SST warming, and (c) historical and (d) future Arctic sea-ice loss.

589 3.5 Response to simultaneous SST and SIC changes

590 We compare the Arctic vs. tropical October-March potential warming contributions of
591 climate feedbacks, changes in atmospheric energy convergence and oceanic heat release in
592 response to historical global SST warming and historical polar sea-ice loss together (i.e., pdSST-
593 pdSIC minus piSST-piSIC; Fig. 14a; referred to as TOTAL) and the sum of the separate responses
594 to historical SST warming (i.e., pdSST-pdSIC minus piSST-pdSIC) and historical polar sea-ice
595 loss (i.e., pdSST-pdSIC minus pdSST-piArcSIC and pdSST-piAntSIC) (Fig. 14b; referred to as
596 SUM). The warming contributions of the lapse rate, water vapor, cloud, and Planck feedbacks in
597 TOTAL match SUM well, with the lapse rate feedbacks making the largest contribution to AA
598 (Fig. 14). Except for CESM2 in TOTAL, the change in atmospheric energy convergence makes
599 roughly equal warming contributions to Arctic and tropical warming from October-March,
600 suggesting that remote SST warming and Arctic sea-ice loss have opposing effects on the

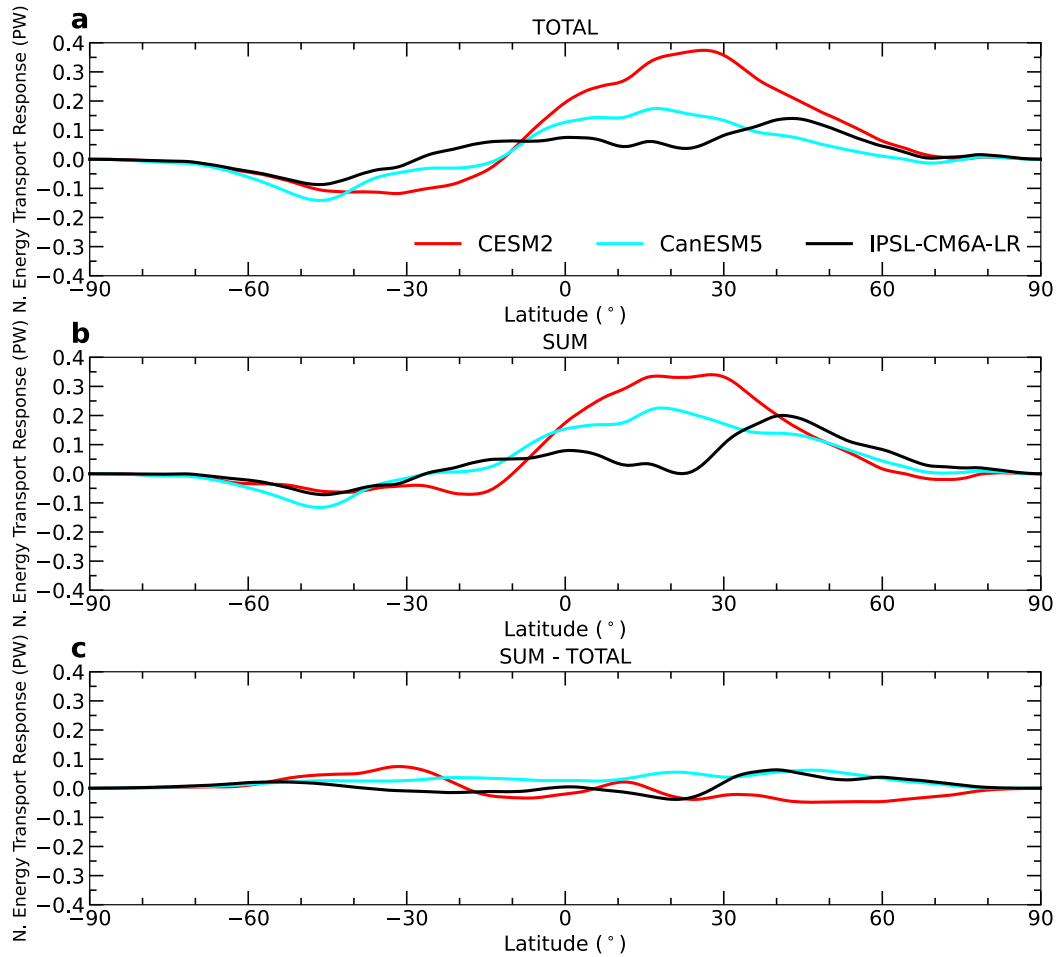
601 horizontal atmospheric energy flux. The oceanic heat release changes in IPSL-CM6A-LR makes
 602 a greater contribution to Arctic than tropical warming, but there are slight discrepancies between
 603 CanESM5 and CESM2 oceanic heat release between TOTAL and SUM. In TOTAL, CanESM5
 604 and CESM2 oceanic heat release changes contributes roughly the same amount to Arctic and
 605 tropical warming; however, CESM2 (CanESM5) produces slightly greater Arctic (tropical)
 606 warming in SUM. The surface albedo feedback is inactive from October-March due to lack of
 607 sunlight and is not a major contributor to large cold-season AA.



608
 609 **Fig. 14.** Inter-model spread in the ensemble mean October-March *potential* warming contributions
 610 (in K) for Arctic (67° - 90° N) and tropical (23.5° S- 23.5° N) surface albedo (α), water vapor (q),
 611 Planck (PL'), lapse rate (LR), and cloud (C) feedbacks, and changes in oceanic heat release ($-\Delta OHU$;
 612 ΔOHU ; positive upwards) and atmospheric energy convergence ($\Delta(-\nabla \cdot \mathbf{F}_A)$) in response to
 613 historical changes in global SST and polar SIC for (a) TOTAL (i.e., global SST and polar SIC
 614 change together) and (b) SUM (i.e., sum of the response to the SST and SIC change separately).

615
 616 The northward atmospheric energy transport response to the SST and SIC perturbations is
 617 similar among TOTAL (Fig. 15a) and SUM (Fig. 15b), with little difference between the two cases
 618 (Fig. 15c). In the tropical regions (i.e., 30° S- 30° N), remote SST warming enhances poleward
 619 atmospheric energy transport by ~ 0.1 - 0.15 PW in the southern hemisphere and ~ 0.1 - 0.35 PW in
 620 the northern hemisphere. Around 60° - 90° N, there is little net change in atmospheric energy

621 transport in response to simultaneous SST and SIC changes, suggesting that remote warming due
 622 to SST changes and local Arctic warming related to sea-ice loss have opposing effects on Arctic
 623 atmospheric energy transport. The similarity of climate feedbacks (Fig. 14) and the atmospheric
 624 energy transport (Fig. 15) response between TOTAL and SUM suggest that the effects of SIC or
 625 SST changes can be linearly separated. In other words, the individual responses to SST or SIC
 626 perturbations approximately sum to the combined influence of changes in SST and SIC.



627
 628 **Fig. 15.** October-March Arctic northward energy transport response (in PW) in response to
 629 historical changes in SST and SIC for (a) TOTAL and (b) SUM, and (c) difference between (b)
 630 and (a).

631
 632 **4. Summary and Conclusions**

633 We investigated the impacts of historical and future Arctic sea-ice loss and global SST
 634 increases on Arctic climate feedbacks, atmospheric energy convergence into the Arctic, and

635 oceanic heat release using PAMIP atmosphere-only simulations. The SST increase with fixed polar
636 sea ice results in relatively uniform global warming with negligible AA for both historical and
637 future cases. In contrast, historical and future Arctic sea-ice loss leads to large Arctic warming
638 with negligible effects south of $\sim 60^\circ\text{N}$, although this may not be the case in fully coupled
639 simulations (Deser et al. 2015). The PAMIP experiments allowed us to separate the response of
640 Arctic climate feedbacks, atmospheric energy convergence, and oceanic heat release to
641 background global warming without AA (as in the SST perturbation runs) or to large AA with
642 negligible warming outside the Arctic (as in the SIC change runs). We also found striking
643 similarities between the historical simulations with both SST and SIC changes together (i.e.,
644 TOTAL), and the sum of the individual responses to the historical SST and polar SIC changes (i.e.,
645 SUM) in terms of Arctic climate feedbacks and atmospheric energy transport response.

646 Under warmer global SSTs without sea-ice loss, Arctic winter oceanic heat release is
647 suppressed leading to weak Arctic cold season warming. Instead, enhanced poleward atmospheric
648 energy convergence rather than increased oceanic heat release becomes the dominant contributor
649 to *small* AA in response to global SST increases with fixed Arctic sea-ice. We also found strong
650 global water vapor feedback in the historical and future SST warming runs, especially in the
651 tropics. However, the combined effects of enhanced atmospheric energy convergence into the
652 Arctic and positive water vapor feedback produce weak Arctic warming without large sea-ice loss
653 and enhanced oceanic heat release. We also found that under global SST warming with fixed Arctic
654 SIC, the Arctic experiences vertically uniform or top-heavy warming, producing a neutral or
655 negative lapse rate feedback. Thus, the lapse rate feedback does not make a large contribution to
656 Arctic warming or AA without the bottom-heavy warming effects of enhanced oceanic energy
657 release due to sea-ice loss. Lastly, Arctic cloud and surface albedo feedbacks responded weakly to
658 warmer global SST with fixed Arctic SIC in the historical and future cases.

659 In contrast, retreating sea ice produces strong bottom-heavy warming and moistening in
660 autumn and winter due to enhanced oceanic energy release in regions with newly exposed water
661 surfaces, as shown in previous studies (Deser et al. 2010; Screen and Simmonds 2010a, b; Boeke
662 and Taylor 2018; Dai et al. 2019; Dai and Jenkins 2023). Strong lower tropospheric warming
663 enhances Arctic positive lapse rate feedback, which greatly contributes to AA during the cold
664 season (e.g., Jenkins and Dai 2021; Dai and Jenkins 2023). Additionally, bottom-heavy moistening

665 in response to Arctic sea-ice loss has little impact on the TOA radiative flux due to its low
666 sensitivity to lower tropospheric water vapor (Shell et al. 2008; Soden et al. 2008; Pendergrass et
667 al. 2018). Instead, enhanced moistening in the mid-upper troposphere, as in the SST warming runs,
668 increases the Arctic TOA radiative forcing by increasing water vapor's LW absorption in the upper
669 troposphere. Arctic surface albedo feedback activates during the sunlit season in response to sea-
670 ice loss but does not significantly raise surface temperatures in summer. We also find reduced
671 poleward atmospheric energy transport in the northern hemisphere mid-high latitudes due to
672 historical and future Arctic sea-ice loss with fixed global SST, consistent with Hahn et al. (2023).

673 Many previous studies have quantified Arctic climate feedback processes in fully coupled
674 model simulations and have suggested that lapse rate feedback is a dominant contributor to AA by
675 comparing its Arctic and tropical warming contributions (Pithan and Mauritsen 2014; Stuecker et
676 al. 2018; Feldl et al. 2020; Hahn et al. 2021). Here, we showed that Arctic lapse rate feedback
677 weakens without sea-ice loss as in the global SST warming with fixed Arctic SIC simulations and
678 activates in the simulations with reduced Arctic sea-ice and enhanced oceanic energy release
679 during the cold season. We emphasize that sea-ice loss, enhanced oceanic heating, and bottom-
680 heavy warming trigger Arctic positive lapse rate feedback, but the effects from the lapse rate
681 feedback in turn amplify Arctic warming resulting from the oceanic energy release, as shown
682 previously (Dai and Jenkins 2023). Therefore, the coupled sea ice loss-lapse rate feedback
683 relationship is an important process underlying large cold-season AA. Further, our results are
684 qualitatively consistent with Jenkins and Dai (2021) and Dai and Jenkins (2023), who showed
685 suppressed lapse rate feedback in a coupled model simulation with fixed sea ice and increasing
686 CO₂.

687 The surface albedo feedback has been suggested to be an important process underlying AA
688 (Hall 2004; Winton 2006) due to its large annual-mean Arctic warming contribution relative to the
689 tropics (Pithan and Mauritsen 2014; Hahn et al. 2021). In response to reduced Arctic sea-ice in the
690 PAMIP runs, surface albedo feedback activates in the summer season when Arctic surface
691 warming and AA are weak and is inactive in winter when AA and Arctic warming are enhanced.
692 This suggests that surface albedo feedback makes a negligible direct contribution to AA and that
693 annual-mean warming contribution analyses may not accurately represent the mechanisms
694 underlying AA, which occurs mainly in the cold season. However, the increased summer

695 absorption of SW radiation may contribute to winter oceanic heat release, thereby indirectly
696 contributing to AA as shown by Dai and Jenkins (2023). We also showed that bottom-heavy
697 moistening related to Arctic sea-ice loss has negligible or slightly negative effects on the TOA
698 radiative flux partly due to near-zero or negative values of the TOA LW water vapor kernel in the
699 Arctic lower troposphere (Pendergrass et al. 2018). Future work may consider estimating water
700 vapor feedback from the surface (rather than TOA) perspective to improve understanding of
701 increased lower tropospheric moistening on the surface radiative flux.

702 We conclude that enhanced atmospheric energy convergence into the Arctic becomes an
703 important process for weak Arctic warming and AA under global SST warming with fixed Arctic
704 SIC. Arctic water vapor feedback also activates in response to remote SST warming rather than
705 local SIC loss likely due to higher sensitivity of water vapor LW effects to upper-tropospheric than
706 lower tropospheric moistening. Sea-ice loss and cold-season oceanic energy release are necessary
707 to produce large bottom-heavy warming and AA, triggering Arctic positive lapse rate feedback.
708 We also found a positive winter cloud feedback in response to sea-ice loss but weak Arctic cloud
709 feedback in the SST warming runs, suggesting that changes in local Arctic surface conditions have
710 a larger influence on Arctic cloud properties than remote processes. The surface albedo feedback
711 activates in response to Arctic sea-ice loss under fixed global SST in the summer months but does
712 not make a large direct contribution to AA due to weak summertime warming in the Arctic. The
713 results from the piSST-piSIC run (i.e., TOTAL), where SIC and SST are changed simultaneously
714 to their historical states, are similar to the sum of piSST-pdSIC, pdSST-piArcSIC, and pdSST-
715 piAntSIC (i.e., SUM) relative to present-day conditions. This suggests that the sum of the separate
716 effects of SST and SIC perturbations approximately equal the combined effects of SST and SIC
717 changes on surface warming, climate feedbacks, and atmospheric energy transport.

718 We recognize that there are limitations associated with atmosphere-only model runs as the
719 ocean is treated as a boundary condition. Ocean-atmosphere coupling and the oceanic component
720 of the poleward energy transport have been shown to play important roles in the atmospheric
721 response to sea-ice loss (Deser et al. 2015; Tomas et al. 2016). Thus, future work may compare
722 our feedback calculations to the results from models with a full-depth dynamical ocean to account
723 for ocean feedbacks. Nevertheless, our results help to untangle the influence of background global

724 warming related to global SST changes or large Arctic warming related to sea-ice loss on Arctic
725 climate feedbacks.

726

727 **Acknowledgements**

728 We thank the contributors to the PAMIP project for designing and running the simulations
729 analyzed in this study.

730 **Author Contributions**

731 M. T. Jenkins performed the analysis for this study, made the figures, and wrote the first draft of
732 the manuscript. A. Dai and C. Deser helped improve the study, the manuscript and the figures.

733 **Funding**

734 This work is supported by the National Science Foundation (grants AGS-2015780 and OISE-
735 1743738). The National Center for Atmospheric Research is supported by the National Science
736 Foundation.

737 **Data Availability Statement**

738 The PAMIP model output used in this study can be downloaded from [https://esgf-
739 node.llnl.gov/search/cmip6/](https://esgf-node.llnl.gov/search/cmip6/).

740 **Ethics Approval**

741 Not applicable.

742 **Consent for Publication**

743 The authors agree to publish the paper in *Climate Dynamics*.

744 **Competing Interests**

745 The authors declare no competing interests.

746

747

748 **References**

- 749 Alexeev VA, Langen PL, Bates JR (2005) Polar amplification of surface warming on an
750 aquaplanet in “ghost forcing” experiments without sea ice feedbacks. *Clim Dyn*, 24:655-
751 666. <https://doi.org/10.1007/s00382-005-0018-3>.
- 752 Barton NP, Veron DE (2012) Response of clouds and surface energy fluxes to changes in sea-ice
753 cover over the Laptev Sea (Arctic Ocean). *Clim Res*, 54:69-84.
754 <https://doi.org/10.3354/cr01101>.
- 755 Bintanja R, Graverson RG, Hazeleger W (2011) Arctic winter warming amplified by the thermal
756 inversion and consequent low infrared cooling to space. *Nat Geosci*, 4:758–761.
757 <https://doi.org/10.1038/ngeo1285>.
- 758 Block K, Mauritsen T (2013) Forcing and feedback in the MPI-ESM-LR coupled model under
759 abruptly quadrupled CO₂. *J Adv Model Earth Syst*, 5:1-16.
760 <https://doi.org/10.1002/jame.20041>.
- 761 Boeke RC, Taylor PC (2018) Seasonal energy exchange in sea ice retreat regions contributes to
762 differences in projected Arctic warming. *Nat Comm*, 9:5017.
763 <https://doi.org/10.1038/s41467-018-07061-9>.
- 764 Boeke RC, Taylor PC, Sejas SA (2021) On the nature of the Arctic’s positive lapse-rate
765 feedback. *Geophys Res Lett*, 48:e2020GL091109.
766 <https://doi.org/10.1029/2020GL091109>.
- 767 Burt MA, Randall DA, Branson MD (2016) Dark warming. *J Climate*, 29:705-719.
768 <https://doi.org/10.1175/JCLI-D-15-0147.1>.
- 769 Cardinale CJ, Rose BEJ (2023) The increasing efficiency of the poleward energy transport into
770 the Arctic in a warming climate. *Geophys Res Lett*, 50:e2022GL100834.
771 <https://doi.org/10.1029/2022GL100834>.
- 772 Cai M (2005) Dynamical amplification of polar warming. *Geophys Res Lett*, 32:L22710.
773 <https://doi.org/10.1029/2005GL024481>.

774 Chung P-C, Feldl N (2023) Sea ice loss, water vapor increases, and their interactions with
775 atmospheric energy transport in driving seasonal polar amplification. J Climate, online.
776 <https://doi.org/10.1175/JCLI-D-23-0219.1>.

777 Colman R, Soden BJ (2021) Water vapor and lapse rate feedbacks in the climate system. Rev
778 Mod Phys, 93:045002. <https://doi.org/10.1103/RevModPhys.93.045002>.

779 Curry JA, Schramm JL, Serreze MC, Ebert EE (1995) Water vapor feedback over the Arctic
780 Ocean. J Geophys Res, 100:14223-14229. <https://doi.org/10.1029/95JD00824>.

781 Dai A, Luo D, Song M, Liu J (2019) Arctic amplification is caused by sea-ice loss under
782 increasing CO₂. Nat Comm, 10:121. <https://doi.org/10.1038/s41467-018-07954-9>.

783 Dai A, Jenkins MT (2023) Relationships among Arctic warming, sea-ice loss, stability, lapse rate
784 feedback, and Arctic amplification. Clim Dyn, 61:5217-5232.
785 <https://doi.org/10.1007/s00382-023-06848-x>.

786 Dai H (2021) Roles of surface albedo, surface temperature, and carbon dioxide in the seasonal
787 variation of Arctic amplification. Geophys Res Lett, 48:e2020GL090301.
788 <https://doi.org/10.1029/2020GL090301>.

789 Davy R, Griewank P (2023) Arctic amplification has already peaked. Environ Res Lett,
790 18:084003. <https://doi.org/10.1088/1748-9326/ace273>.

791 Deser C, Tomas R., Alexander M, Lawrence D (2010) The seasonal atmospheric response to
792 projected Arctic sea ice loss in the late twenty-first century. J Climate, 23:333-351.
793 <https://doi.org/10.1175/2009JCLI3053.1>.

794 Deser C, Tomas RA, Sun L (2015) The role of ocean-atmosphere coupling in the zonal-mean
795 atmospheric response to Arctic sea ice loss. J Climate, 28:2168-2186.
796 <https://doi.org/10.1175/JCLI-D-14-00325.1>.

797 Eastman R, Warren SG (2010) Interannual variations of Arctic cloud types in relation to sea ice.
798 J. Climate 23:4216-4232. <https://doi.org/10.1175/2010JCLI3492.1>.

799 England MR, Eisenman I, Lutsko NJ, Wagner TJ (2021) The recent emergence of Arctic
800 amplification. *Geophys Res Lett*, 48:e2021GL094086.
801 <https://doi.org/10.1029/2021GL094086>.

802 Fasullo JT, Trenberth KE (2008) The annual cycle of the energy budget. Part I: Global mean and
803 land-ocean exchanges. *J Climate*, 21:2297-2312.
804 <https://doi.org/10.1175/2007JCLI1935.1>.

805 Feldl N, Anderson BT, Bordoni S (2017a) Atmospheric eddies mediate lapse rate feedback and
806 Arctic amplification. *J Climate*, 30:9213-9224. <https://doi.org/10.1175/JCLI-D-16-0706.1>.

807

808 Feldl N, Bordoni S, Merlis TM (2017b) Coupled high-latitude climate feedbacks and their
809 impact on atmospheric heat transport. *J Climate*, 30:189-201.
810 <https://doi.org/10.1175/JCLI-D-16-0324.1>.

811 Feldl N, Po-Chedley S, Singh HKA, Hay S, Kushner PJ (2020) Sea ice and atmospheric
812 circulation shape the high-latitude lapse rate feedback. *npj Climate and Atmospheric*
813 *Science*, 3:41. <https://doi.org/10.1038/s41612-020-00146-7>.

814 Ghatak D, Miller J (2013) Implications for Arctic amplification of changes in the strength of the
815 water vapor feedback. *J Geophys Res Atmos*, 118:7569-7578.
816 <https://doi.org/10.1002/jgrd.50578>.

817 Gong T, Feldstein S, Lee S (2017) The role of downward infrared radiation in the recent Arctic
818 winter warming trend. *J Climate*, 30:4937-4949. <https://doi.org/10.1175/JCLI-D-16-0180.1>.

819

820 Goosse H, Kay JE, Armour KC, Bodas-Salcedo A, Chepfer H, Docquier D, et al. (2018)
821 Quantifying climate feedbacks in polar regions. *Nat Comm*, 9:1919.
822 <https://doi.org/10.1038/s41467-018-04173-0>.

823 Hay S, Kushner PJ, Blackport R, McCusker KE, Oudar T, Sun L, et al. (2022) Separating the
824 influences of low-latitude warming and sea-ice loss on northern hemisphere climate
825 change. *J Climate*, 35:2327-2349. <https://doi.org/10.1175/JCLI-D-21-0180.1>.

826 Hahn LC, Armour KC, Zelinka MD, Bitz CM, Donohoe A (2021) Contributions to polar
827 amplification in CMIP5 and CMIP6 models. *Front Earth Sci*, 9:710036.
828 <https://doi.org/10.3389/feart.2021.710036>.

829 Hahn LC, Armour KC, Battisti DS, Eisenman I, Bitz CM (2022) Seasonality in Arctic warming
830 driven by sea ice effective heat capacity. *J. Climate*, 35:1629-1642.
831 <https://doi.org/10.1175/JCLI-D-21-0626.1>.

832 Hahn LC, Armour KC, Battisti DS, Donohoe A, Fajber R (2023) Seasonal changes in
833 atmospheric heat transport to the Arctic under increased CO₂. *Geophys Res Lett*,
834 50:e2023GL105156. <https://doi.org/10.1029/2023GL105156>.

835 Hall A (2004) The role of surface albedo feedback in climate. *J Climate*, 17:1550-1568.
836 [https://doi.org/10.1175/1520-0442\(2004\)017%3C1550:TROSAF%3E2.0.CO;2](https://doi.org/10.1175/1520-0442(2004)017%3C1550:TROSAF%3E2.0.CO;2).

837 Henry M, Merlis TM, Lutsko NJ, Rose BEJ (2021) Decomposing the drivers of polar
838 amplification with a single-column model. *J Climate*, 34:2355-2365.
839 <https://doi.org/10.1175/JCLI-D-20-0178.1>.

840 Hwang Y-T, Frierson DMW (2010) Increasing atmospheric poleward energy transport with
841 global warming. *Geophys Res Lett*, 37:L24807. <https://doi.org/10.1029/2010GL045440>.

842 Hwang Y-T, Frierson DMW, Kay JE (2011) Coupling between Arctic feedbacks and changes in
843 poleward energy transport. *Geophys Res Lett*, 38:L17704.
844 <https://doi.org/10.1029/2011GL048546>.

845 Janoski TP, Previdi M, Chiodo G, Smith KL, Polvani LM (2023) Ultrafast Arctic amplification
846 and its governing mechanisms. *Environ. Res.: Climate*, 2:035009.
847 <https://doi.org/10.1088/2752-5295/ace211>.

848 Jenkins M, Dai A (2021) The impact of sea-ice loss on Arctic climate feedbacks and their role
849 for Arctic amplification. *Geophys Res Lett*, 48:e2021GL094599.
850 <https://doi.org/10.1029/2021GL094599>.

851 Jenkins MT, Dai A (2022) Arctic climate feedbacks in ERA5 reanalysis: Seasonal and spatial
852 variations and the impact of sea-ice loss. *Geophys Res Lett*, 49:e2022GL099263.
853 <https://doi.org/10.1029/2022GL099263>.

854 Jenkins MT, Dai A, Deser C (2023) Seasonal variations and spatial patterns of Arctic cloud
855 changes in association with sea-ice loss during 1950-2019 in ERA5. J Climate,
856 <https://doi.org/10.1175/JCLI-D-23-0117.1>.

857 Kay JE, Gettelman A (2009) Cloud influence on and response to seasonal Arctic sea-ice loss. J
858 Geophys Res, 114:D18204. <https://doi.org/10.1029/2009JD011773>.

859 Kay JE, L'Ecuyer T, Chepfer H, Loeb N, Morrison A, Cesana G (2016) Recent advances in
860 Arctic cloud and climate research. Curr Clim Change Rep, 2:159-169.
861 <https://doi.org/10.1007/s40641-016-0051-9>.

862 Kumar A, Perlwitz J, Eischeid J, Quan X, Xu T, Zhang T, et al. (2010) Contribution of sea ice
863 loss to Arctic amplification. Geophys Res Lett, 37:L21701.
864 <https://doi.org/10.1029/2010GL045022>.

865 Liang Y-C, Kwon Y-O, Frankignoul C, Gastineau G, Smith KL, Polvani LM, et al. (2023) The
866 weakening of the stratospheric polar vortex and the subsequent surface impacts as
867 consequences to Arctic sea-ice loss. J Climate, 37:309-333. <https://doi.org/10.1175/JCLI-D-23-0128.1>.

869 Linke O, Quaas J, Baumer F, Becker S, Chylik J, Dahlke S, et al. (2023a) Constraints on
870 simulated past Arctic amplification and lapse rate feedback from observations. Atmos.
871 Chem. Phys. 23:9963–9992. <https://doi.org/10.5194/acp-23-9963-2023>.

872 Linke O, Feldl N, Quaas J (2023b) Current-climate sea ice amount and seasonality as constraints
873 for future Arctic amplification. Environ Res: Climate, 2:045003.
874 <https://doi.org/10.1088/2752-5295/acf4b7>.

875 Liu Y, Key JR, Liu Z, Wang X, Vavrus SJ (2012) A cloudier Arctic expected with diminishing
876 sea ice. Geophys Res Lett, 39:L05705. <https://doi.org/10.1029/2012GL051251>.

877 Merlis TM, Henry M (2018) Simple estimates of polar amplification in moist diffusive energy
878 balance models. J Climate, 31:5811-5824. <https://doi.org/10.1175/JCLI-D-17-0578.1>.

879 Middlemas EA, Kay JE, Medeiros BM, Maroon EA (2020) Quantifying the influence of cloud
880 radiative feedbacks on Arctic surface warming using cloud locking in an Earth system
881 model. Geophys Res Lett, 47:e2020GL089207. <https://doi.org/10.1029/2020GL089207>.

882 Monroe EE, Taylor PC, Boisvert LN (2021) Arctic cloud response to a perturbation in sea ice
883 concentration: The north water polynya. *J Geophys Res Atmos*, 126:e2020JD034409.
884 <https://doi.org/10.1029/2020JD034409>.

885 Morrison AL, Kay JE, Chepfer H, Guzman R, Yettella V (2018) Isolating the liquid cloud
886 response to recent Arctic sea ice variability using spaceborne lidar observations. *J*
887 *Geophys Res Atmos*, 123:473-490. <https://doi.org/10.1002/2017JD027248>.

888 Morrison AL, Kay JE, Frey WR, Chepfer H, Guzman R (2019) Cloud response to Arctic sea ice
889 loss and implication for future feedback in the CESM1 climate model. *J Geophys Res*
890 *Atmos*, 124:1003-1020. <https://doi.org/10.1029/2018JD029142>.

891 Oort AH, Vonder Haar TH (1976) On the observed annual cycle in the ocean-atmosphere heat
892 balance over the northern hemisphere. *J Phys Oceanogr*, 6:781-800.
893 [https://doi.org/10.1175/1520-0485\(1976\)006%3C0781:OTOACI%3E2.0.CO;2](https://doi.org/10.1175/1520-0485(1976)006%3C0781:OTOACI%3E2.0.CO;2).

894 Palm SP, Strey ST, Spinhirne J, and Markus T (2010) Influence of Arctic sea-ice extent and
895 polar cloud fraction and vertical structure and implications for regional climate. *J*
896 *Geophys Res*, 115:D21209. <https://doi.org/10.1029/2010JD013900>.

897 Pendergrass AG, Conley A, Vitt FM (2018) Surface and top-of-atmosphere radiative feedback
898 kernels for CESM-CAM5. *Earth Sys Sci Data*, 10:317-324. [https://doi.org/10.5194/essd-](https://doi.org/10.5194/essd-10-317-2018)
899 [10-317-2018](https://doi.org/10.5194/essd-10-317-2018).

900 Perlwitz J, Hoerling M, Dole R (2015) Arctic tropospheric warming: causes and linkages to
901 lower latitudes. *J Climate*, 28:2154-2167. <https://doi.org/10.1175/JCLI-D-14-00095.1>.

902 Pithan F, Mauritsen T (2014) Arctic amplification dominated by temperature feedbacks in
903 contemporary climate models. *Nat Geosci*, 7:181-184.
904 <https://doi.org/10.1038/NGEO2071>.

905 Previdi M, Janoski TP, Chiodo G, Smith KL, Polvani LM (2020) Arctic amplification: A rapid
906 response to radiative forcing. *Geophys Res Lett*, 47:e2020GL089933.
907 <https://doi.org/10.1029/2020GL089933>.

908 Roe GH, Feldl N, Armour KC, Hwang Y-T, Frierson DMW (2015) The remote impacts of
909 climate feedbacks on regional climate predictability. *Nat Geosci*, 8:135-139.
910 <https://doi.org/10.1038/NGEO2346>.

911 Screen JA, Simmonds I (2010a) The central role of diminishing sea ice in recent Arctic
912 temperature amplification. *Nature*, 464:1334-1337. <https://doi.org/10.1038/nature09051>.

913 Screen JA, Simmonds I (2010b) Increasing fall-winter energy loss from the Arctic Ocean and its
914 role in Arctic temperature amplification. *Geophys Res Lett*, 37:L16707.
915 <https://doi.org/10.1029/2010GL044136>.

916 Screen JA, Deser C, Simmonds I, Tomas R (2014) Atmospheric impacts of Arctic sea-ice loss,
917 1979-2009: Separating forced change from atmospheric internal variability. *Clim Dyn*,
918 43:333-344. <https://doi.org/10.1007/s00382-013-1830-9>.

919 Schweiger AJ, Lindsay RW, Vavrus S, Francis JA (2008) Relationships between Arctic sea ice
920 and clouds during autumn. *J. Climate*, 21:4799-4810.
921 <https://doi.org/10.1175/2008JCLI2156.1>.

922 Sejas SA, Taylor PC, Cai M (2018) Unmasking the negative greenhouse effect over the Antarctic
923 Plateau. *npj Climate and Atmospheric Science*, 1:17. [https://doi.org/10.1038/s41612-018-](https://doi.org/10.1038/s41612-018-0031-y)
924 [0031-y](https://doi.org/10.1038/s41612-018-0031-y).

925 Serreze MC, Barry RG (2011) Processes and impacts of Arctic amplification: A research
926 synthesis. *Global and Planetary Change*, 77:85-96.
927 <https://doi.org/10.1016/j.gloplacha.2011.03.004>.

928 Shell KM, Kiehl JT, Shields CA (2008) Using the radiative kernel technique to calculate climate
929 feedbacks in NCAR's community atmospheric model. *J Climate*, 21:2269–2282.
930 <https://doi.org/10.1175/2007JCLI2044.1>.

931 Smith DM, Screen JA, Deser C, Cohen J, Fyfe JC, García-Serrano J, et al. (2019) The polar
932 amplification model intercomparison project (PAMIP) contribution to CMIP6:
933 Investigating the causes and consequences of polar amplification. *Geosci Model Dev*,
934 12:1139-1164. <https://doi.org/10.5194/gmd-12-1139-2019>.

935 Soden BJ, Held IM, Colman R, Shell KM, Kiehl JT, Shields CA (2008) Quantifying climate
936 feedbacks using radiative kernels. *J. Climate*, 21:3504-3520.
937 <https://doi.org/10.1175/2007JCLI2110.1>.

938 Soldatenko S (2021) Effects of global warming on the poleward heat transport by non-stationary
939 large-scale atmospheric eddies, and feedbacks affecting the formation of the Arctic
940 climate. *J Mar Sci Eng*, 9:867. <https://doi.org/10.3390/jmse9080867>.

941 Stuecker MF, Bitz CM, Armour KC, Proistosescu C, Kang SM, Xie S-P, et al. (2018) Polar
942 amplification dominated by local forcing and feedbacks. *Nat Clim Change*, 8:1076-1081.
943 <https://doi.org/10.1038/s41558-018-0339-y>.

944 Sun L, Perlwitz J, Hoerling M (2016) What caused the recent “Warm Arctic, Cold Continents”
945 trend pattern in winter temperatures? *Geophys Res Lett*, 43:5345-5352.
946 <https://doi.org/10.1002/2016GL069024>.

947 Taylor PC, Kato S, Xu K-M, Cai M (2015) Covariance between Arctic sea ice and clouds within
948 atmospheric state regimes at the satellite footprint level. *J Geophys Res Atmos*,
949 120:12656-12678. <https://doi.org/10.1002/2015JD023520>.

950 Taylor PC, Hegyi BM, Boeke RC, Boisvert LN (2018) On the increasing importance of air-sea
951 exchanges in a thawing Arctic: A review. *Atmosphere*, 9:41.
952 <https://doi.org/10.3390/atmos9020041>.

953 Taylor PC, Boeke RC, Boisvert LN, Feldl N, Henry M, Huang Y, et al. (2022) Process drivers,
954 inter-model spread, and the path forward: A review of amplified Arctic warming. *Front.*
955 *Earth Sci.*, 9:758361. <https://doi.org/10.3389/feart.2021.758361>.

956 Taylor PC, Monroe E (2023) Isolating the surface type influence on Arctic low-clouds. *J*
957 *Geophys Res Atmos*, 128:e2022JD038098. <https://doi.org/10.1029/2022JD038098>.

958 Tomas RA, Deser C, Sun L (2016) The role of ocean heat transport in the global climate
959 response to projected Arctic sea ice loss. *J Climate*, 29:6841-6859.
960 <https://doi.org/10.1175/JCLI-D-15-0651.1>.

961 Trenberth KE, Solomon A (1994) The global heat balance: heat transports in the atmosphere and
962 ocean. *Clim Dyn*, 10:107-134. <https://doi.org/10.1007/BF00210625>.

963 Trenberth KE (1997) Using atmospheric budgets as a constraint on surface fluxes. J Climate,
964 10:2796-2809. [https://doi.org/10.1175/1520-](https://doi.org/10.1175/1520-0442(1997)010%3C2796:UABAAC%3E2.0.CO;2)
965 [0442\(1997\)010%3C2796:UABAAC%3E2.0.CO;2](https://doi.org/10.1175/1520-0442(1997)010%3C2796:UABAAC%3E2.0.CO;2).

966 Vavrus S (2004) The impact of cloud feedbacks on Arctic climate under greenhouse forcing. J
967 Climate, 17:603-615. [https://doi.org/10.1175/1520-](https://doi.org/10.1175/1520-0442(2004)017%3C0603:TIOCF0%3E2.0.CO;2)
968 [0442\(2004\)017%3C0603:TIOCF0%3E2.0.CO;2](https://doi.org/10.1175/1520-0442(2004)017%3C0603:TIOCF0%3E2.0.CO;2).

969 Virgin JG, Smith KL (2019) Is Arctic amplification dominated by regional radiative forcing and
970 feedbacks: Perspectives from the world-avoided scenario. Geophys Res Lett, 46:7708-
971 7717. <https://doi.org/10.1029/2019GL082320>.

972 Walsh JE (2014) Intensified warming of the Arctic: Causes and impacts on middle latitudes.
973 Global and Planetary Change, 117:52-63.
974 <https://doi.org/10.1016/j.gloplacha.2014.03.003>.

975 Wetherald RT, Manabe S (1988) Cloud feedback processes in a general circulation model. J
976 Atmos Sci, 45:1397-1415. [https://doi.org/10.1175/1520-](https://doi.org/10.1175/1520-0469(1988)045%3C1397:CFPIAG%3E2.0.CO;2)
977 [0469\(1988\)045%3C1397:CFPIAG%3E2.0.CO;2](https://doi.org/10.1175/1520-0469(1988)045%3C1397:CFPIAG%3E2.0.CO;2).

978 Winton M (2006) Amplified Arctic climate change: What does surface albedo feedback have to
979 do with it? Geophys Res Lett, 29:4473-4485. <https://doi.org/10.1029/2005GL025244>.

980 Zhou S-N, Liang Y-C, Mitevski I, Polvani LM (2023) Stronger Arctic amplification produced by
981 decreasing, not increasing, CO₂ concentrations. Environ Res: Climate, 2:045001.
982 <https://doi.org/10.1088/2752-5295/aceea2>.